Pathways towards high energy aqueous rechargeable batteries

Dan Yang,[a,b,†] Yanping Zhou,[c,†] Hongbo Geng,[a,*] Chuntai Liu,[d] Bo Lu,[d] Xianhong Rui,[b,*] Qingyu Yan[e,*]

[a]School of Materials Engineering, Changshu Institute of Technology, Changshu, Jiangsu 215500, China. E-mail: genghonhbo@126.com (H. Geng)

[b]Guangzhou Key Laboratory of Low-Dimensional Materials and Energy Storage Devices, School of Materials and Energy, Guangdong University of Technology, Guangzhou 510006, China. E-mail: xhrui@gdut.edu.cn (X. Rui)

[c]Key Laboratory of Wireless Power Transmission of Ministry of Education, College of Electronics and Information Engineering, Sichuan University, Chengdu 610065, China

[d]Key Laboratory of Materials Processing and Mold, Ministry of Education, Zhengzhou University, Zhengzhou 450002, China.

[e]School of Materials Science and Engineering, Nanyang Technological University, 639798, Singapore. E-mail: alexyan@ntu.edu.sg (Q. Yan)

[†]D. Yang and Y. Zhou contributed equally to this study.

Abstract: Aqueous rechargeable metal batteries (ARMBs) represent one type of energy storage technology with high theoretical energy densities, low cost and better safety. Their practical applications are hindered by the narrow voltage window of the aqueous electrolytes, limited efficiency in the intercalation/deintercalation of the metal ions (especially for the multivalent ions) and dissolution/structural variation of the electrodes in aqueous electrolytes. Effective strategies have been developed to address the above issues and significantly advanced performance and mechanistic understanding of the aqueous system. In this review, we highlight the representative strategies in achieving high-energy ARMBs, i.e., aqueous rechargeable Li/Na/K/Zn/Mg/Al ion batteries. Strategies in optimizing the composition/structure of conventional anodes and cathodes, progress of "water-in-salt" electrolyte, and novel ion storage mechanisms other than the intercalation chemistry will be discussed. It is expected that this review can provide a comprehensive overview of the status of the ARMBs and enlighten more research work that tackle the unsolved bottleneck issues.

Keywords: aqueous battery; alkaline metal; ion intercalation; high-energy; water-in-salt electrolyte

1. Introduction

Reliable energy storage technology is imperative to provide us the energy on demand and reduce our reliance on the fossil fuels. Lithium ion batteries (LIBs) are undoubtedly playing a dominant role in the global energy market by powering many consumer electronics. Now it is enjoying an increasing market share in the section of transportation as a major driving force of most electric vehicles. With respect to further breakthrough of current LIB technology, aside from the moderate energy density (limited endurance or driving range of

electronic devices or vehicles), one major concern is the utilization of flammable organic electrolyte, which is considered to be responsible for several catastrophic fires or explosions. The quest for safe battery system with high power and energy density have stimulated the extensive research in exploiting alternative battery technologies.

Rechargeable aqueous battery system is highly attractive. The history of using water as solvent in the battery can be dated back to the 19th century. Conventional batteries, such as Ni/Cd, Pb/Acid, and Ni/MH all use aqueous electrolyte. It is not until recent decades that different metal ion batteries step back to the sight of researchers (**Fig. 1**). Despite organic solvent has revived the LIB technology by expanding the voltage window to 3 V and above, unremitting efforts are still being devoted to the exploration of aqueous rechargeable metal batteries (ARMBs) with high energy density (i.e., high cell voltage and specific capacity). One grand challenge is that their voltage is limited by the electrochemical stability of the aqueous electrolyte. The stable voltage window for water is close to 1.23 V, which is much lower than that of organic electrolytes (> 3 V). But in practical ARMBs, this voltage window is also largely determined by the overpotentials required to initiate the water decomposition, i.e., the pH and concentration of the aqueous electrolytes and the property of electrode materials. The potentials where electrolysis of water takes place varied with pH of the aqueous electrolyte, e.g., the potential of hydrogen gas evolution from water decreases at a rate of 0.059 V per pH unit [1]. The voltage window could be wider in the vicinity of electrodes due to the local pH change, especially in neutral electrolytes. The $LiNO_3$ electrolyte showed widest stability window at neutral pH which decreased with increasing pH values [2]. An acidic–alkaline double electrolyte was developed to decrease HER potential in the anode side with basic electrolyte, and increase OER potential in the cathode compartment with the acid electrolyte, resulting in a high-voltage Zn/$KMnO_4$ aqueous cell [3]. As well-reported in the nonaqueous LIBs, the solid-electrolyte interphase (SEI) layer formed in the

organic electrolyte could protect the electrode surface and extend the voltage window. Similar concept has been applied in the design of aqueous batteries. For example, with addition of certain surfactants, such as sodium dodecyl sulfate (SDS) into the aqueous electrolytes, the voltage window can be expanded to 2.5 V via the formation of a hydrophobic protective layer onto the electrode surface [4]. As a result, the aqueous rechargeable Na/Zn hybrid battery delivered a high energy density of 170 Wh kg^{-1}. On the other hand, the development of the "water-in-salt" electrolyte has successfully expanded the stability window of aqueous electrolyte up to 3 V and led to a high energy density of 100 Wh kg^{-1} [5, 6]. By eliminating the free water molecules in the highly concentrated electrolytes, direct interaction between electrode and water can be avoided. A protective layer was further formed on the surface of the electrode with reduction of the salt anions, and this has effectively increased the stability of electrolytes and led to a much higher voltage window as compared to the diluted ones. To date, the "water-in-salt" electrolyte has been widely applied in the design and fabrication of high-energy ARMBs, including the Na/K/Zn/Mg/Al ion batteries etc. [7-9].

Besides, the electrode materials for ARMBs should be carefully selected to avoid electrolysis of aqueous electrolyte. One important criterion in selecting electrodes for ARMBs is that their working potentials should be within the electrochemical stability window of aqueous electrolyte. Otherwise, water will decompose through the hydrogen evolution reaction (HER) and oxygen evolution reaction (OER) and the electrodes can hardly realize the redox reactions. Besides, since the voltage window of aqueous electrolyte is related with the interaction between electrode materials and water, the property of electrode materials, e.g., their chemical stability, solubility in the electrolyte and resistance towards the electrolysis, should be carefully considered. In recent years, various types of cathode and anode materials have been developed for the ARMBs [10-15]. For example, layered Mn_5O_8

nanoparticles with a well-ordered hydroxylated interphase demonstrated high resistance to gas evolution reactions and the aqueous Na-ion half-cell showed a stable 2.5 V potential window [16]. The co-intercalated water molecules in the bilayer $Zn_{0.25}V_2O_5 \cdot nH_2O$ electrode could buffer the high charge density of divalent Zn^{2+} ions and reduce the activation energy for charge transfer at the electrode interface, and the aqueous Zn ion battery displayed a specific energy of ~250 Wh kg^{-1} (cathode only) [13]. Recently, an impressive breakthrough is made by introduction of the new chemistry other than the traditional intercalation chemistry into aqueous battery system [17]. With the anionic-redox reaction of halide anions (Br^- and Cl^-)$C_{3.5}[Br_{0.5}Cl_{0.5}]$), the LIB full cell delivered a high capacity of 243 mAh g^{-1} at the voltage of 4.2 V with an energy density as high as 304 Wh kg^{-1}.

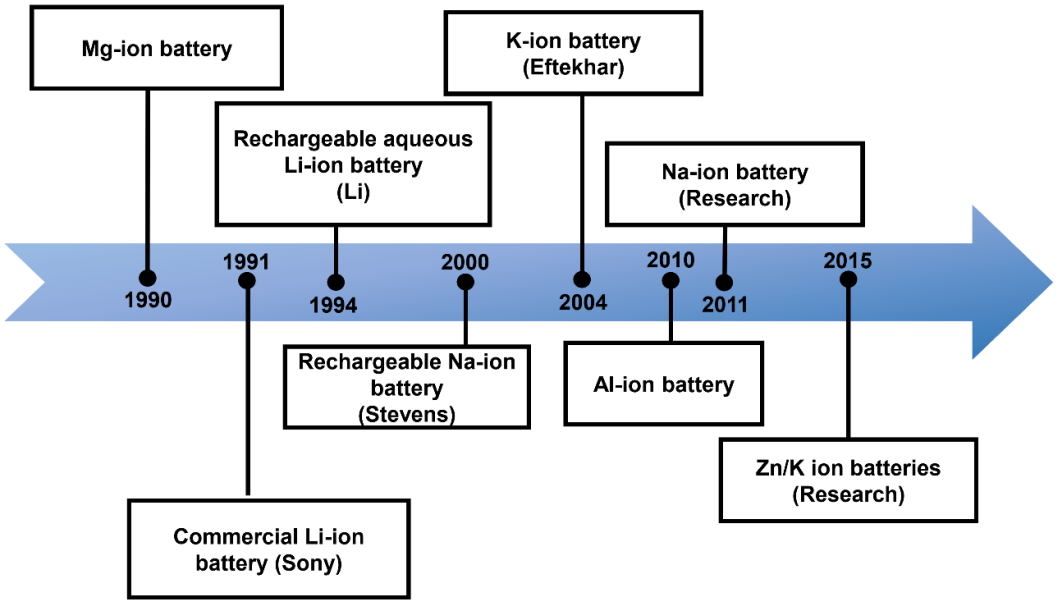

Fig. 1. Development history of the aqueous metal batteries.

Due to so many literatures reported on the battery system using aqueous electrolyte, here we only make an in-depth and comprehensive overview over the current aqueous rechargeable battery system based on alkaline metal ions (Li/Na/K/Zn/Mg/Al). Conventional nickel or lead based aqueous batteries, metal-air and redox-flow batteries will not be covered

in this review. **Table 1** summarizes the physical and electrochemical properties of typical metal ions. Similar with the electrochemistry in the nonaqueous system, energy storage in the aqueous electrolyte is realized through migration and intercalation/deintercalation of metal ions into the host electrode materials, where the ion diffusion kinetics are even faster in aqueous media. In contrary to the highly reactive metal Li, Na and K, metals like Zn, Mg and Al are relative more stable in the aqueous electrolyte, which simplifies the electrode fabrication and cell manufacturing process. The multivalent metal ions (Zn^{2+}, Mg^{2+}, Al^{3+}) can also transfer more electrons and show higher energy density in theory. But the challenge is the stronger electrostatic interactions between these multivalent ions and the host structures, resulting in poor insertion kinetics and unstable output voltage.

Table 1. Physical/electrochemical properties of different metal ions.

Ion	**Radius (nm)**	**Voltage (V vs. SHE)**	**Volumetric capacity ($mAh\ cm^{-3}$)**	**Gravimetric capacity ($mAh\ g^{-1}$)**
Li^+	0.076	-3.05	2044	3829
Na^+	0.102	-2.71	1128	1165
K^+	0.138	-2.93	609	610
Zn^{2+}	0.074	-0.76	5854	820
Mg^{2+}	0.065	-2.36	3882	2234
Al^{3+}	0.054	-1.66	8046	2980

There have been papers providing comprehensive comparison and discussion on the charge storage mechanisms, design guidelines of the electrode materials, and optimization of the battery configurations and so on [18-22]. Here, to differ from the perspectives provided in earlier review articles and provide specific insights on how to boost energy density of this kind of battery system, we highlight representative strategies in achieving high specific capacity and voltage, which translate into the high energy of ARMBs.

2. Aqueous rechargeable batteries

To date, the development of rechargeable aqueous batteries is still facing many challenges. Firstly, despite can be tuned by tailoring electrodes or adding additives, the voltage of the dilute aqueous electrolytes are still far below the one of organic electrolytes (mostly above 3 V). Secondly, the mechanism of interaction between metal ions and active materials in the aqueous electrolyte is complicated. The co-insertion of H^+ and the exchange of metal ions with H^+ during the cycling has been reported to be responsible for the low specific capacity of the aqueous system [23]. The dissolution of electrodes in the aqueous electrolyte is another issue affecting the capacity and stability. Moreover, concentration, PH, dissolved oxygen, as well as additives in the electrolyte all affect the output and stability of the aqueous battery systems.

2.1 Development of "water-in-salt" electrolyte.

In 2015, Suo et al. introduced the "water-in-salt" (WIS) concept to the aqueous lithium battery system [5, 6]. They manipulated the inter-phase chemistry on the electrode surface by dissolving lithium bis (trifluoromethane sulfonyl) imide (LiTFSI) at extremely high concentrations. The highly concentrated electrolyte (21 m) provided a stable voltage window up to 3 V and the full aqueous battery constructed from the $LiMn_2O_4/Mo_6S_8$ couple showed an open circuit voltage (OCV) of 2.3 V with a high energy density of 84 Wh kg^{-1} (or 100 Wh kg^{-1} if eliminating the loss in SEI formation). With the dense-packing niobium tungsten oxide ($Nb_{16}W_5O_{55}$ and $Nb_{18}W_{16}O_{93}$) as the anode, the full cell showed a high volumetric energy of ~200 Ah L^{-1} [24]. The exceptional performance was originated from the decomposition of the salt anion on the anode, which resulted in the formation of a dense solid electrolyte interface (SEI). Further research by Dubouis et al. reveals that it is the hydroxides generated during the hydrogen evolution reaction that chemically react with TFSI and catalyze the formation of a fluorinated solid–electrolyte interphase (SEI) that prevents further water reduction.[25]

Recently, with the advanced transmission x-ray microscopy (TXM) techniques, Lin et al. identify that besides of delaying the water decomposition, the WIS electrolyte can suppress the mechanical damage to the electrode network and dissolution of the electrode.[26] On the other hand, similar to the concept of WIS electrolyte, Yamada et al. proposed an eutectic systems comprised of hydrate melt of Li salts. The lithium battery with this electrolyte shows a high energy density of >130 Wh kg^{-1} and high voltage (∼2.3–3.1 V)[27]. The voltage window of WIS electrolyte was enlarged to 2.5 V by introducing a second lithium salt in the almost saturated LiTFSI solution, known as the "water-in-bisalt" (WIBS) [28]. The WIBS system consisting of 21 m LiTFSI and 7 m LiOTf (in total 28 m Li^{+}) achieved an energy density of 100 Wh kg^{-1} based on the total mass of the electrode (the full cell was coupled with $LiMn_2O_4$ and TiO_2). Lukatskaya et al. further lowered the cost of concentrated electrolyte by employing 32 m KCH_3COO (KOAc) mixed with 8m LiOAc ($Li_{0.2}K_{0.8}OAc{\cdot}1.3H_2O$) as the aqueous electrolyte.[29] The $TiO_2/LiMn_2O_4$ full cell as-assembled delivered an operation voltage of 2.5 V. It is the development of WIS electrolyte that brings about the reviving of aqueous metal batteries and makes them strong competitor towards the nonaqueous counterparts in terms of energy density. By using super-concentrated electrolytes, the oxygen and hydrogen evolution in water can be effectively suppressed and the solvation structure has been changed with ion aggregation. As a result, the electrochemical stability window in such aqueous system has been expanded and enabled high-voltage and high-energy aqueous batteries with a broader selection of electrode materials. To date, this concentrated electrolyte system has been widely utilized in various aqueous metal batteries. The composition and performance optimization, cost, and more in-depth mechanistic understanding of this electrolyte system are hot topics at current stage[30-32].

2.2 Aqueous rechargeable lithium batteries (ARLBs)

Usage of aqueous electrolyte can effectively address the issues related to thermal runaway and simplify the battery management system, thereby reducing the manufacturing cost of the battery [33]. Coating the Li metal anode with a gel polymer electrolyte (GPE) and LISICON film could enable the direct implementation of Li metal in aqueous electrolytes [34, 35]. The ARLB system pairing the $LiFePO_4$ and Li metal in Li_2SO_4 electrolyte displayed an average discharge voltage of 3.32 V, leading to a high energy density of 342 Wh kg^{-1}. Besides of Li-based anodes, Xu et al. employed carbon coated TiP_2O_7 as anode for ARLBs and the full cell paired with $LiMn_2O_4$ delivered a capacity of 83.5 mAh g^{-1} [36]. $FePO_4$ and amorphous $FePO_4 \cdot 2H_2O$ have been used as anodes [37]. Despite the olivine $FePO_4$ showed larger capacity than the amorphous counterparts, the amorphous $FePO_4 \cdot 2H_2O$ showed much superior stability over long time cycling. Though the electrochemical stability window of electrolyte can be expanded to 3 V, the energy density of the ARLBs still cannot compete with that of organic LIBs. The gap is generated by the phenomenon known as "cathodic challenge". When the electrode potential is polarized to 0.5 V, an interface with water molecules adsorbing with hydrogens will disrupt the SEI layer formed on the anode and thereby excludes application of high-energy anode materials such as graphite, lithium metal and shield and impedes further improvement of energy density for ARLBs. By coating the graphite or lithium anode surface with a fluorinated ether HFE (1,1,2,2-Tetrafluoroethyl-2',2',2'-trifluoroethyl) mixed with the LiTFSI, a SEI layer can be formed on the anode surface and this has created a 4 V ARLB [38].

Regarding the cathode materials for ARLBs, a major part of the research is devoted to the modification of existing cathode materials used for LIBs. Nanostructuring or surface modification over the electrode surface with inorganic materials or polymer coating has proved to be effective in improving performance of the LIBs [39-45]. Coating the spinel

$LiMn_2O_4$ surface with LaF_3 can promote diffusion of Li^+ ions and reduce dissolution of Mn^{2+} in the aqueous electrolyte and enhance the electrochemical performance [46]. $LiFePO_4$ with 1 wt% AlF_3 coating on the surface delivered a high discharge capacity of 132 mAh g^{-1} [47]. Since the decay of electrode performance is related with oxygen presented in the electrolyte, materials that can survive under high PH value and high oxygen concentration can make a difference in the battery performance. Representatively, Yao's group has spotted the organic Quinone with remarkable stability as electrodes and the ARLBs showed much higher capacity as compared to the regular inorganic electrodes [48]. Limited by the intercalation chemistry, the conventional transition-metal-oxide cathode can only achieve capacities less than 200 mAh g^{-1}, which becomes the bottleneck to the further advance in the energy density of the ARLBs. In contrary to conventional rocking-chair battery, which relies on the insertion/de-insertion of single metal ions, the dual-ion-batteries (DIBs) could achieve a higher capacity by supporting the simultaneous intercalation of anions and cations from both the positive and negative electrodes [49]. Anions (such as Cl^-, $PF6^-$, $TFSI^-$, and $AlCl_4^-$) were investigated in the DIBs with graphite as both the positive and anodes [50]. To further improve their energy density, Hao et al. recently introduced a novel hybrid $LiFePO_4$ (LFP)/graphite electrode, which can realize intercalation/deintercalation of both Li^+ and PF_6^- over a broad voltage ranged from 2.5 to 4 V (**Fig. 2**a-c) [51]. By replacing the conductive amorphous carbon with graphite that can realize ion intercalation/de-intercalation, the full cell assembled from LFP/graphite-20% cathode and a graphite anode realized an energy density of 176.7 Wh kg^{-1} (**Fig. 2**d).

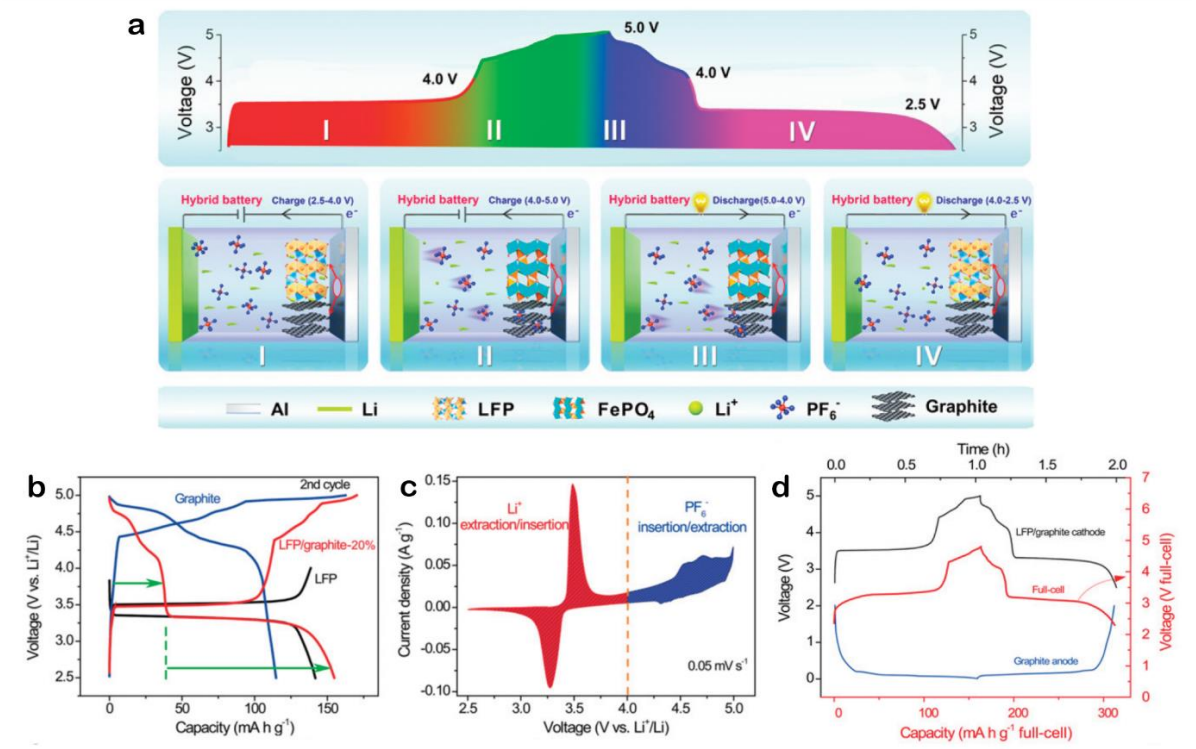

Fig. 2 Hybrid LFP/graphite battery. (a) Scheme illustration of the battery in half-cell configuration. (b) Charge-discharge profiles at the second cycle. (c) Cyclic voltammograms (CV) of the LFP/graphite at 0.5 mV s^{-1}. (d) Charge-discharge curves in a full cell. Reprinted with copyright from Ref. [51].

Besides of altering battery configurations, exploration of novel reaction chemistry in the traditional electrode materials represents another effective pathway towards high-energy ARLBs.[42] Significantly, halogen ions have been introduced into graphite to form a solid graphite intercalation compounds $C_{3.5}[Br_{0.5}Cl_{0.5}]$) [17]. With the anionic-redox reaction of halide anions (Br^- and Cl^-) (**Fig. 3**a and b), Br^0 and Cl^0 were stabilized by sequential intercalation into the graphite host and such halogen conversion-intercalation chemistry led to a high capacity of 243 mAh g^{-1} at the voltage of 4.2 V (vs. Li/Li^+) in an aqueous gel polymer electrolyte. The energy density of the LIB full cell reached 460 Wh kg^{-1} (304 Wh kg^{-1} with electrolyte), far exceeding the previous aqueous and even non-aqueous LIBs (**Fig. 3**c).

Performance of ARLBs developed recently is summarized in **Table 2**.

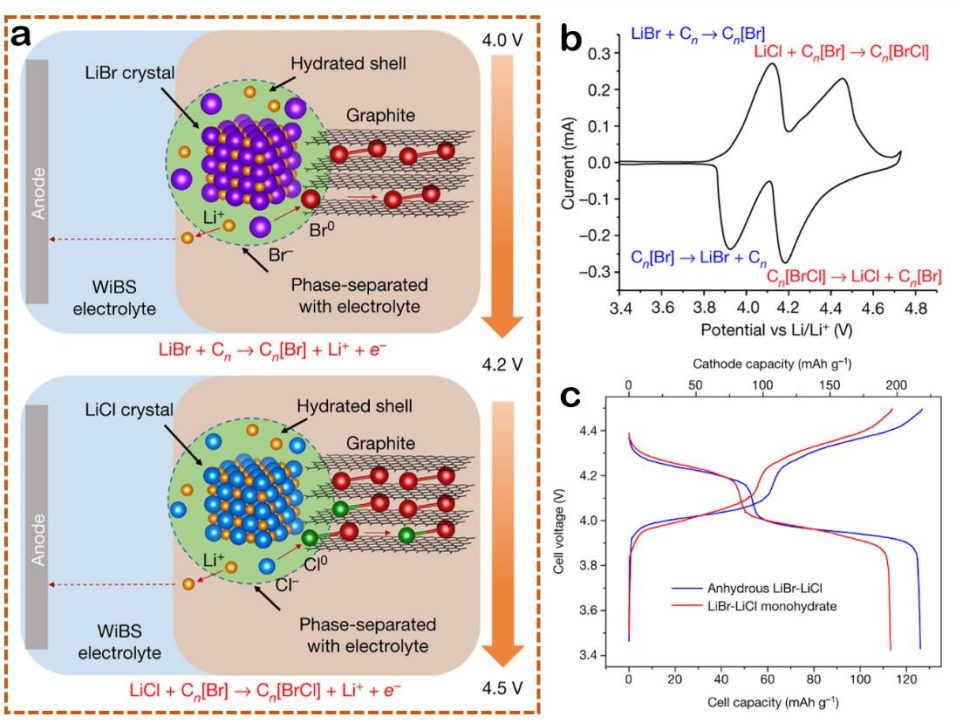

Fig. 3. The ARLB with conversion–intercalation chemistry. (a) The proposed conversion-intercalation mechanism. (b) CV curve of the $(LiBr)_{0.5}(LiCl)_{0.5}$-graphite (LBC-G) cathode at 0.5 mV s^{-1}. (c) The charge-discharge curves of the full cell consisted of the LBC-G cathodes HFE/poly (ethylene oxide)-protected graphite anodes. Reprinted with copyright from Ref.[17].

Table 2. Performance of recent ARLBs.

Cell type	Electrolyte (solvent: water)	Operating Voltage (V)	Capacity (mAh g^{-1}@C rate)	Energy density (Wh kg^{-1})	Ref.
Cathode: $LiMn_2O_4$ Anode: Olivine $FePO_4$	15 m LiTFSI	3.4	163@0.2 C		[37]
Cathode: Spinel $LiMn_2O_4$ Anode: $LiTi_2(PO_4)_3$@ carbon	Saturated Li_2SO_4	1.6	112.5@0.2 C		[52]
Cathode: $LiMn_2O_4$ Anode: $Na_{1.1}Ti_{1.9}Fe_{0.1}(PO_4)_3$/C	Saturated Li_2SO_4	1.6	103.1@5 C		[53]
Cathode: $LiMn_2O_4$ Anode: $LiTi_2(PO_4)_3$	1 M $LiNO_3$		98@3 C		[54]

Cathode: $LiMn_2O_4$ Anode: Na-doped $LiTi_2(PO_4)_3$@carbon	2 M Li_2SO_4	~1.6	98.5@0.2 C		[55]
Cathode: Carbon cloth/$LiCoO_2$ Anode: Carbon cloth/$LiTi_2(PO_4)_3$/C	Saturated Li_2SO_4	1.5	130.3@1 C		[56]
Cathode: $LiFePO_4$/C Anode: Platinum	1 M Li_2SO_4	~0.18 (vs Ag/AgCl)	163.5@0.1 C		[57]
Cathode: $LiMn_2O_4$ Anode: Polyimide/activated carbon	5 M $LiNO_3$	1.21	42@0.2 Ag^{-1}	51	[58]
Cathode: $LiMn_2O_4$ Anode: TiP_2O_7/expanded graphite	1 M Li_2SO_4	1.4	42@0.1 Ag^{-1}	60	[59]
Cathode: AlF_3-coated $LiFePO_4$ Anode: Activated carbon composite	1 M Li_2SO_4	0.15 (vs Ag/AgCl)	132 @ 1 C		[47]
Cathode: $LiMn_2O_4$ Anode: N-doped carbon coated $LiTi_2(PO_4)_3$	Saturated Li_2SO_4	1.5	122.4 @ 0.2 C		[60]
Cathode: $LiMn_2O_4$ Anode: $LiTi_{1.7}Sn_{0.3}(PO_4)_3$/C	Saturated Li_2SO_4	~1.5	118.9 @ 0.2 C		[61]
Cathode: $LiNi_{0.5}Mn_{1.5}O_4$ Anode: Mo_6S_8	1 M HTFSI	2.5	~58@0.5 C	126	[62]
Cathode: $LiVPO_4F$ Anode: $LiVPO_4F$	25 m LiTFSI	2.4	58.1@2 C	141	[63]
Cathode: $LiMn_2O_4$ Anode: CNTs modified $LiTi_2(PO_4)_3$	2 M Li_2SO_4	~1.6	~115@0.5 C		[64]
Cathode: $LiMn_2O_4$ Anode: $LiTi_2(PO_4)_{2.88}F_{0.12}$	2 M Li_2SO_4	~1.6	45@2 C	66.7	[65]
Cathode: $LiMn_2O_4$ Anode: Graphene/$NaTi_2(PO_4)_3$/C	Saturated Li_2SO_4	~1.5	107.8@0.5 C		[66]
Cathode: $LiMn_2O_4$ Anode: Carbon-coated $LiTi_2(PO_4)_3$	2 M Li_2SO_4	1.5	124@1 C	26–31 mWh cm^{-3}	[67]
Cathode: $LiMn_2O_4$ Anode: $LiTi_2(PO_4)_3$@carbon	2 M Li_2SO_4	1.52	107.6@0.2 C		[68]
Cathode: $LiMn_2O_4$ Anode: MWCNTs@S@PPy	Saturated LiAc	1.25	250@0.5 Ag^{-1}	110	[69]

2.2 Aqueous rechargeable sodium batteries (ARSBs)

Although the LIBs have been maturely developed for portable electronics and electric vehicles, their further progress still face great challenges associated with the cost and safety concerns. As a result, ARSBs with similar intercalation electrochemistry to LIBs but much lower cost has been considered.

At first, the conventional anode graphite has proven not suitable to be applied for Na^+ ion storage. While further research demonstrated that other carbonaceous materials with

tailored structure can still serve as anodes for ARSBs. For example, hydrophobic few-layer graphene was employed as the capacitive anode and due to its hydrophobic nature, the anode surface preferably adsorb metals ions instead of H^+ ions, which reduced the parasitic H_2 evolution reaction [70]. Inspired by the successful practice of Quinone derivatives in the lithium ion storage, biomolecules with diverse chemical structures and approximate redox potential to H_2 evolution threshold have been explored. Long et al. proposed an ARSB system with the 9,10-anthroquinone alizarin derived from plant as the anode [71]. With the capability of the biomolecules to self-assemble into nanowires, the electrode delivered a high capacity of 233.1 mAh g^{-1} and by pairing with polypyrrole (PPy).

The cathode materials for ARSBs can be categorized into three types, i.e., metal oxides, Prussian blue analogues (PBAs), and NASICON compounds [72-78]. Jiang et al. have proposed that crystal water in the PBA structure can increase their average voltage and reduce the volume change during the cycling. They further identified four PBA cathodes, $Na_2CoMn(CN)_6$, $Na_2NiMn(CN)_6$, $Na_2CuMn(CN)_6$, and $Na_2ZnMn(CN)_6$ as the potential cathodes to achieve high energy density ARSBs [79]. One of the advantages associated with the PBA electrodes is the feasibility to replace metal ions coordinated with C in the crystal structure. Wheeler et al. have explored the feasibility of lowering the redox potential of PBA cathode by replacing the C-coordinated Fe with Mn and Cr to form cubic manganese hexacyanochromate (MnHCCr) enriched with defects (**Fig. 4**a-c), lowering the potential to 0 V and -0.86 V vs SHE , respectively (**Fig. 4**d) [80].

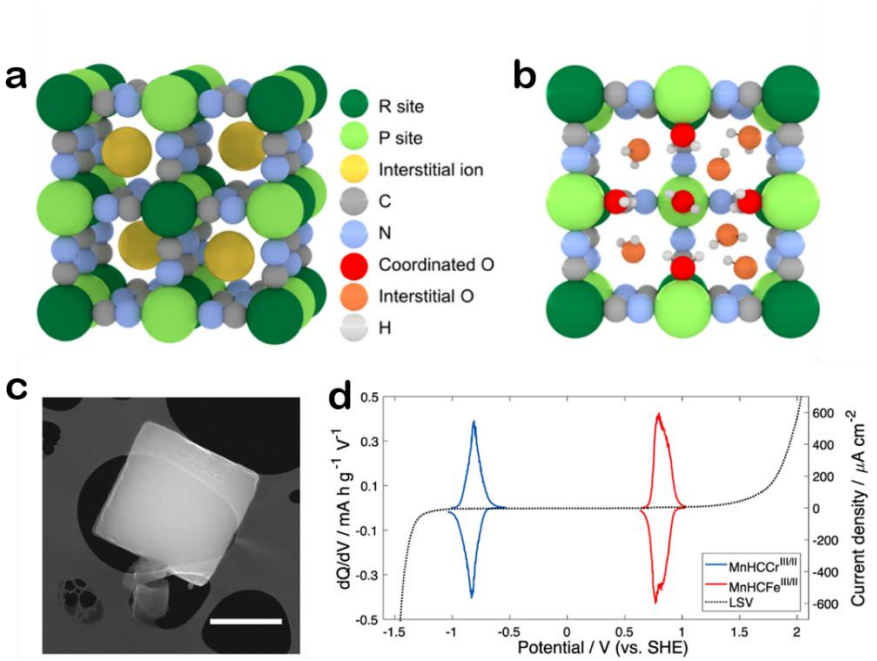

Fig. 4. ARSB with manganese hexacyanochromate (MnHCCr) cathode. (a) Crystal structure of the "ideal" PBAs. (b) The crystal structure of PBA with defects and water. (c) Morphology of the MnHCCr electrode. (d) Linear sweep voltammetry (LSV) of the water-in-salt (WiS) electrolyte. Reprinted with copyright from Ref. [80].

To develop electrolyte suitable for the ARSB, Kuhnel et al. discovered sodium bis(fluorosulfonyl)imide (NaFSI) with a high solubility in water (up to 37 m) and a high room-temperature conductivity of up to 90 mS cm^{-1} [81]. Most water molecules are simultaneously formed as the first solvation sheath with strong coordination to the cation, and the highest occupied molecular orbital of the water molecules shifted to more negative energy, offering a high voltage of 2.6 V. However, one challenge of using highly concentrated electrolyte is that it tends to crystallize in the room temperature. Through replacing a fraction of the symmetric anions with the asymmetric anions (using sodium (fluorosulfonyl)(trifluoromethylsulfonyl)imide (NaFTFSI) as the ternary electrolyte), the water-in-salt electrolyte can be kinetically stabilized with an expanded liquidise temperature

range. With this concept, the cell assembled with $NaTi_2(PO_4)_2$ and $Na_3(VOPO_4)_2F$ electrodes reaches a specific energy of 64 Wh kg^{-1} with an operating voltage of 2 V. Moreover, the cell can be operated below -10 ^oC with 74% capacity retention at 0.2 C [38, 51, 82]. Despite of the encouraging results from the concentrated electrolytes, concerns have also been raised about their high cost and toxicity (fluorinated). To tackle these concerns, researchers have explored cheaper inorganic salts with high solubility in water. Jiang et al. developed a new electrolyte composed of polyethylene glycol (PEG)/H_2O/$NaClO_4$ with a low H^+ concentration [83]. Presence of PEG in the electrolyte assisted formation of the PEG-Na^+ interface on the electrode, which provides the pathway for the access of Na^+ ions and prevents dissolution of cathode into the electrolyte. Han et al. developed a highly concentrated WIS electrolyte by dissolving 32 m potassium acetate (KAc) with 8 m sodium acetate (NaAc). The electrochemical window was expanded, but in the full cell assembled from $Na_2MnFe(CN)_6$ (NMHCF) and $NaTi_2(PO_4)_3$/C (NTP/C) electrodes, the irreversible sodiation/desodiation was observed, which led to the low capacity of the cell [84]. Coupled with the same electrodes, i.e., NMHCF as the cathode and NTP as the anode, Nakamoto et al. used highly concentrated $NaClO_4$ (17 m), and achieved a voltage of 1.4 V (**Fig. 5**a and b) [85]. Later, they replaced the NTP with $KMn[Cr(CN)_6]$ (KMHCC) with lower redox potentials and the battery presented a much higher voltage of 2.8 V (**Fig. 5**c and d). [74] Lee et al. identified that the 17 m $NaClO_4$ could assist formation of the surface layer composed of Na_2CO_3 and NaOH [86]. The full cell with $Na_4Fe_3(PO_4)_2(P_2O_7)$/NTP as electrodes showed a 2.7 V voltage window, leading to a high energy density of 36 Wh kg^{-1}.

For comparison, the electrochemical performance of the ARSBs developed in recent two years have been summarized and listed in **Table 3.**

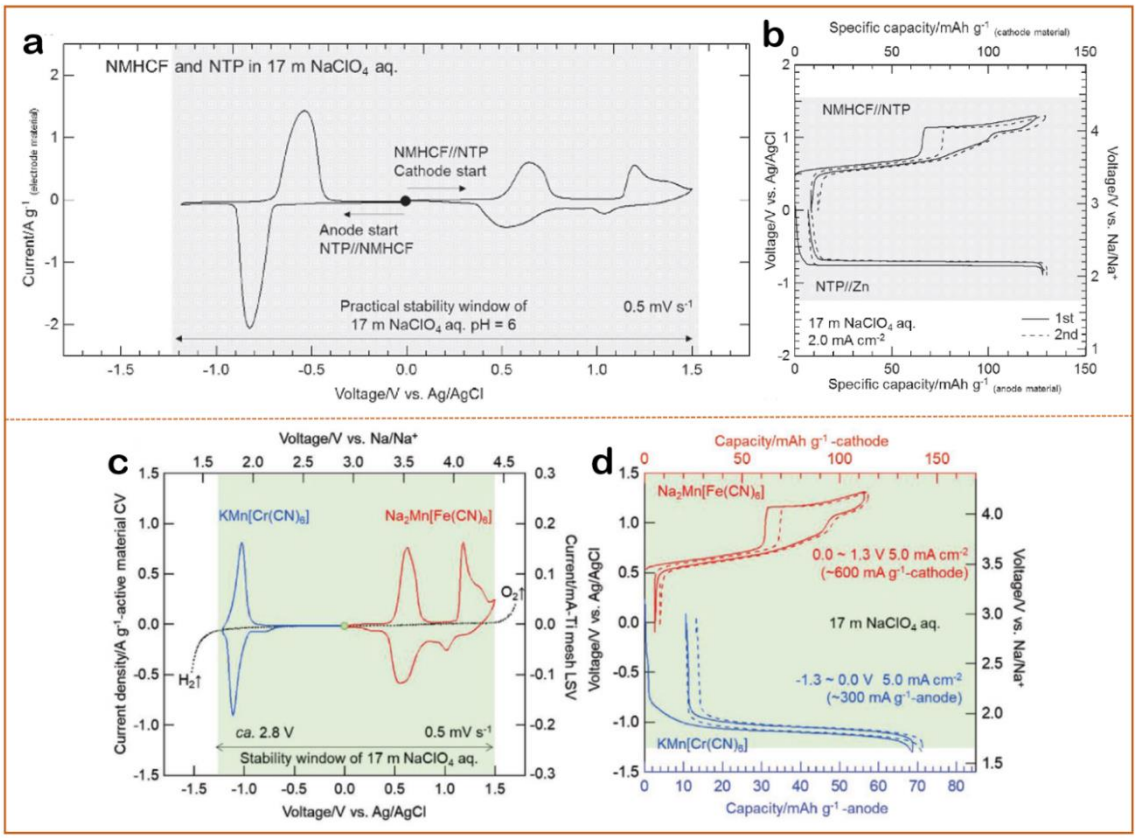

Fig. 5. Effect of anodes. (a) CV profiles of NMHCF and NTP in 17 m $NaClO_4$. (b) Charge-discharge curves of NMHCF//NTP full cell and NTP//Zn half-cell in 17 m $NaClO_4$. Reprinted with copyright from Ref. [85]. (c) CV curves of NMHCF and KMHCC in 17 m $NaClO_4$. (d) Charge/discharge curves of NMHCF and KMHCC half cells. Reprinted with copyright from Ref. [74].

Table 3. Composition and performance of the recently developed ARSBs.

Cell type	Electrolyte (solvent: water)	Operating Voltage (V)	Capacity (mAh g^{-1}@C rate)	Energy density (Wh kg^{-1})	Ref.
Cathode: $Na_2VTi(PO_4)_3$/C Anode: $Na_2VTi(PO_4)_3$/C	1 M Na_2SO_4	~1.2	58@2 C	~34	[87]
Cathode: $Na_2VTi(PO_4)_3$ Anode: $Na_2VTi(PO_4)_3$	1 M Na_2SO_4	~ 1.2	56@1 C	~30	[76]
Cathode: PBA Anode: Pt foil	0.5 M Na_2SO_4 + 5 M H_2SO_4		90@1.2 C		[88]
Cathode: $Na_2VO_x[Fe(CN)_6]$ Anode: Pt wire	1 M $LiNO_3$/3 M $NaNO_3$/3 M KNO_3 + 3.6 M H_2SO_4	~0.9	~80@30 C		[89]
Cathode: $Na_{2/3}Ni_{1/4}Mn_{3/4}O_2$ Anode: $NaTi_2(PO_4)_3$/graphite	1 M Na_2SO_4/Li_2SO_4 (mole ratio as 2:2)	~1.2	~60@0.1 C	36	[90]
Cathode: $Na_{0.44}MnO_2$ Anode: $NaTi_2(PO_4)_3$@C	1 M Na_2SO_4	~1.1	43@0.1 A g^{-1}	25.7 mWh cm^{-3}	[91]

Cathode: $Na_{0.44}MnO_2$ Anode: aligned $NaV_3(PO_4)_3$ nanofiber	1 M Na_2SO_4	~0.5	~120@1 C		[92]
Cathode: $Na_4Fe_3(PO_4)_2(P_2O_7)$ Anode: $NaTi_2(PO_4)_3$	1 M $NaClO_4$	~1.0	~44@1 C	36	[86]
Cathode: $Na_{0.44}MnO_2$ Anode: Pt foil	1 M Na_2SO_4	1.3	77.2@0.1 A g^{-1}		[93]
Cathode: MnHCCr (PBAs) Anode: MnHCFe	37 m NaFSI	2.5	62@10 μA cm^{-2}		[80]
Cathode: $Na_4MnV(PO_4)_3$ Anode: $NaTi_2(PO_4)_3$	1 M Na_2SO_4	~1.3	97@10 C	130	[94]
Cathode: $Na_{0.66}Mn_{0.66}Ti_{0.34}O_2$ Anode: $Na_{1.5}Ti_{1.5}Fe_{0.5}(PO_4)_3$	5 M $NaClO_4$		105.6@2 C		[95]
Cathode: $K_2Zn_3[Fe(CN)_6]_2 \cdot 9H_2O$ Anode: $NaTi_2(PO_4)_3$	Poly(vinyl alcohol) -$NaClO_4$ gel	~1.6	0.56 mAh cm^{-2} @0.5 mA cm^{-2}	0.92 mWh cm^{-2}	[96]
Cathode: m-NiHCF Anode: $NaTi_2(PO_4)_3$@C	5 M $NaClO_4$	1.4	61.4@100 mA g^{-1}	86	[97]
Cathode: $Na_{0.66}[Mn_{0.66}Ti_{0.34}]O_2$ Anode: $NaTi_2(PO_4)_3$	9.26 m $NaCF_3SO_3$	1.0	31@0.2 C	31	[98]
Cathode: $Na_{0.44}MnO_2$ Anode: $FePO_4 \cdot 2H_2O$	1 M Na_2SO_4	0.7	70@3 C		[99]
Cathode: $Na_2Mn[Fe(CN)_6]$ Anode: $KMn[Cr(CN)_6]$	17 m $NaClO_4$	~2.3	~35@5 C	58	[74]
Cathode: $(Na_{4-\delta}Fe_3(PO_4)_2P_2O_7)$ Anode: activated carbon	1 M Na_2SO_4	3.0	84@1 C		[100]
Cathode: Na_2FePO_4F Anode: $NaTi_2(PO_4)_3$	17 m $NaClO_4$	0.7	85@1 $mAcm^{-2}$	30	[77]
Cathode: PB/MoS_2 Anode: Steel sheet	1 M Na_2SO_4	~0.5 (vs Ag/AgCl)	177@1 A g^{-1}		[101]
Cathode: N-doped porous carbon Anode: $NaTi_2(PO_4)_3$@C	1 M Na_2SO_4		~90@0.5 A g^{-1}		[102]

2.3 Aqueous rechargeable potassium batteries (ARKBs)

ARKBs are intriguing because the natural abundance and smaller solvation size of the K ions. Metal K is highly reactive and not suitable to be directly used as anode in aqueous systems, but the K-C anode is more favourable with higher operation potentials, and the concern of forming metal dendrite is less as compared to the Li–C and Na–C counterparts [103, 104]. A theoretical value of 279 mAh g^{-1} can be obtained with formation of KC_8. The main challenge of using carbon as anode is the drastic volume change (~61%) generated during the potassiation process and this hinders practical commercialization of carbon-based anodes. Alloy-type anode materials, like Sn/C composite, delivered a moderate capacity as compared to the carbonaceous materials[105]. Zhang et al. further demonstrated Sn_4P_3/C

composite as a novel anode material for potassium ion batteries (KIBs). The electrode could deliver a reversible capacity of 384.8 mA h g^{-1} at 50 mA g^{-1} and a good rate capability of 221.9 mA h g^{-1}, even at 1 A g^{-1} [106].

To date, the most widely explored electrode materials for ARKBs is the Prussian Blue Analogues (PBAs) because of their open-framework structure to the large interstitial sites and 3D channel that allows fast insertion/extraction of metal ions [107, 108]. Ren et al. reported an ultrafast ARKB with the potassium-rich mesoporous nickel ferrocyanide (II) ($K_2NiFe(CN)_6 \cdot 1.2H_2O$) as electrode. Such electrode can achieve superior capacity retention after long-term cycling and only takes 4.1 s for one charge or discharge. In fact, the main challenge of the PBA electrodes are their low capacity and low voltage. The typical capacity of the PBAs for ARKBs is lower than 125 mAh g^{-1}. Prussian white analogues ($K_{1.93}Fe[Fe(CN)_6]_{0.97} \cdot 1.82H_2O$) with high crystallinity achieved a capacity of 142 mAh g^{-1} at 75 mA g^{-1} [109]. With regulation over the composition of the PB analogue, the Ni and Co doped PB composite cathode achieved delivers a high initial capacity of 86 mAh g^{-1} with a retention of 98 % after 50 cycles [110].

The organic compounds are promising electrode candidates due to flexibility in tailoring their structure and they are able to promote multi-electron transfer. So far, polymers such as poly(anthraquinonyl sulfide) (PAQS) oligo(anthraquinonyl sulfide) (OAQS) and oligohexane(anthraquinone sulfide) (OHAQS) have been explored for ARKBs [48, 111]. The challenges in the organic electrodes is their high solubility in the aqueous electrolyte. Not only the molecular structure but also the molecular weight plays a decisive role in determining the stability of such electrode. Polymerization is an effective strategy to suppress dissolution of electrodes. Liu et al. controlled the polymerization degree of the poly(1,4-anthraquinone) (P14AQ) and with higher polymerization degree, the dissolution of electrode can be effectively suppressed, but the capacity would be lower due to less active sites

exposed. A hybrid cell composed of P14AQ/Co–Ni$(OH)_2$ delivered an energy density of 93 Wh kg^{-1} at 1040 W kg^{-1} with the operating temperature ranging from -30 ^oC to 25 ^oC [112]. Recently, Jiang et al. reported an ARKB system with a high energy density of 80 Wh kg^{-1} over a wide operating temperature from -20 to 60 ^oC [113]. Fe-substituted Mn-rich Prussian blue $K_xFe_yMn_{1-y}[Fe(CN)_6]_w \cdot zH_2O$ cathode (KFeMnHCF-3565) (**Fig. 6**a), an organic 3,4,9,10-perylenetetracarboxylic diimide anode and the 22 m KCF_3SO_3 water-in-salt electrolyte were integrated into a powerful ARKB system. The highly concentrated water-in-salt electrolyte depressed the solubility of organic anodes and ensured stable cycling of the cell (**Fig. 6**b and c). The substitution of Fe ions in the KMnHCF altered the phase transition behaviour during the electrochemical process. In contrary to the two-phase transition in the KMnHCF electrode, the Fe-substituted electrode underwent a phase transition between monoclinic and cubic structure (**Fig. 6**d) and showed improved electronic and K^+-ion conductivities (**Fig. 6**e-f) [113].

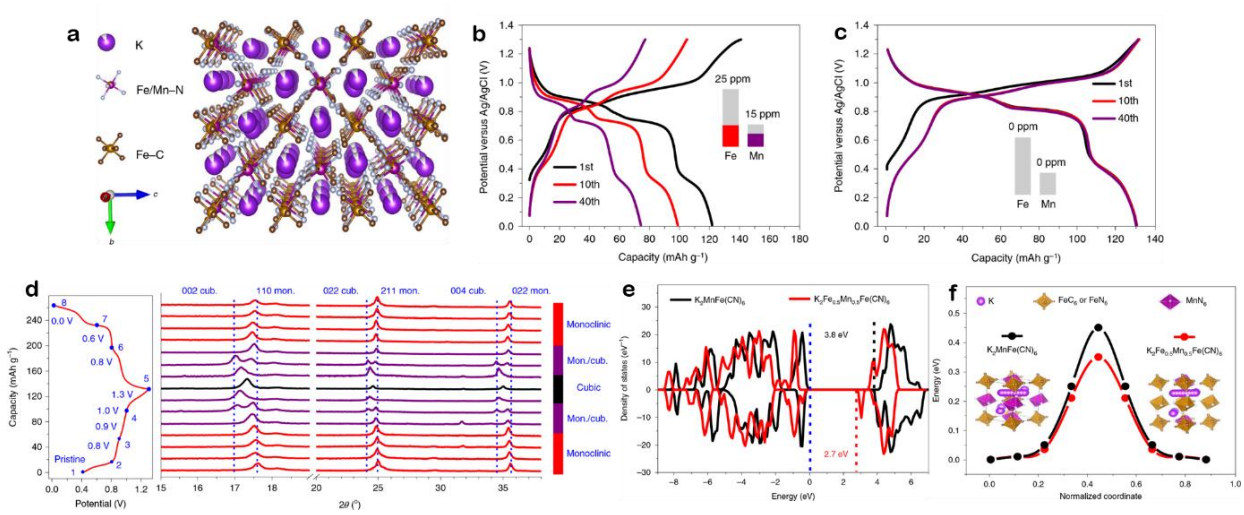

Fig. 6. (a) The typical structure of the KFeMnHCF-3565 electrode. Charge-discharge profiles of the electrode in (b) 1 M and (c) 22 m KCF_3SO_3 electrolyte. (d) Ex situ XRD patterns of the electrodes at different states during the 1st cycle. (e and f) First-principle calculation results: density of states (e) and migration barrier (f) of K^+ in $K_2MnFe(CN)_6$ and Fe-substituted $K_2Fe_{0.5}Mn_{0.5}Fe(CN)_6$ electrodes. Reprinted with permission from Ref. [113].

2.4 Aqueous rechargeable zinc batteries (ARZBs)

In recent years, considerable research has been devoted to the development of Zn-based battery technologies, especially aqueous rechargeable zinc batteries (ARZBs). Metal Zn is cheaper and more naturally abundant than Li. In contrary to Li/Na/K, which are reactive towards the aqueous electrolyte, metal Zn is very stable and can be directly applied as anode for the aqueous batteries, rendering a much simplified process in the design and manufacturing of the Zn-based technology [114]. One bottleneck associated with the Zn anode is the uneven distribution and precipitation of the zincate intermediates. Dendrites tend to form on the surface of the anode, which not only leads to fluctuation of the energy output, causes low utilization efficiency of the material, but also poses risks in penetrating the packages.

With proper design in electrode and electrolyte, the dendrite growth and hydrogen evolution issues can be significantly addressed [115-117]. With the nanostructuring of the electrode, the electrochemical reactivity was improved, but accompanied by more severe corrosion due to increased surface area. With introduction of other metal species, the conductivity of Zn anode can be improved, and current distribution can be more uniform. On the other hand, wrapping Zn or ZnO with a thin protective layer is also a good practice to isolate Zn anode from the corrosive electrolyte [118]. For example, an ion-sieving carbon shell was introduced onto surface of ZnO nanoparticles. With the protection of the carbon layer, the dissolution of the Zn was mitigated and the passivation of ZnO was also alleviated, which addresses the passivation and dissolution problem simultaneously [119]. Similarly, with TiN_xO_y shell on the ZnO nanorod surface, the battery delivered a high capacity of 508 mAh g^{-1} (Zn) with stable performance for over 64 days [120]. Zhao et al. have elevated the nucleation barrier and restricts the 2D diffusion pathway of Zn^{2+} on the anode surface and enabled dendrite-free Zn anode with polyamine as the buffering layer [121]. By coating with nano-porous $CaCO_3$, the stripping/plating behaviour of the Zn anode was effectively regulated and led to increased discharge capacity of the Zn anode [122]. In a recent report, Zheng et al. electrodeposited Zn on a graphene-coated stainless-steel electrode and regulated formation of the Zn plates with preferential orientation. As such, the batteries show excellent cycling stability and reversibility for over thousands of cycles.[123] The evolution of hydrogen on the Zn surface consumes extra electrolyte, generates bubbles and converts active Zn into inactive and insulating surface. This decreases the usable capacity and is responsible for the self-discharge of the Zn-based battery. On the other hand, with polymers additives such as PMMA, polypyrrole, and polyaniline, and surfactants such as PEG and SDS into electrolyte, the dissolution of Zn in electrolyte can be reduced [124, 125].

The 3D Zn anode with rich porosity in the microstructure has suppressed the formation of dendrite and elevated performance of the batteries. A discharge capacity as high as 730 mAh g^{-1} was achieved with this design. Recently, the same group further optimized the sponge structure with increased solid volume fraction from 20% (**Fig. 7**a-c) to 30% (**Fig. 7**d-f) and a high bulk density of 2.1 g cm^{-3}. With increased interconnectivity in the dense sponge, the mechanical strength of the anode was improved, with a 55% increase in the modulus of toughness. With the high utilization efficiency (**Fig. 7**g), the Ag-Zn cell achieved a high capacity of 780 mAh g^{-1}, translating to a high energy density of 204 Wh kg^{-1} (**Fig. 7**h) [124]. By depositing Zn onto chemically etched 3D copper substrate, the Zn anode showed fast electrochemical kinetics and allows more uniform deposition/stripping of Zn. The full cell delivered a high capacity of 364 mAh g^{-1} with long-term stability up to 350 h [126].

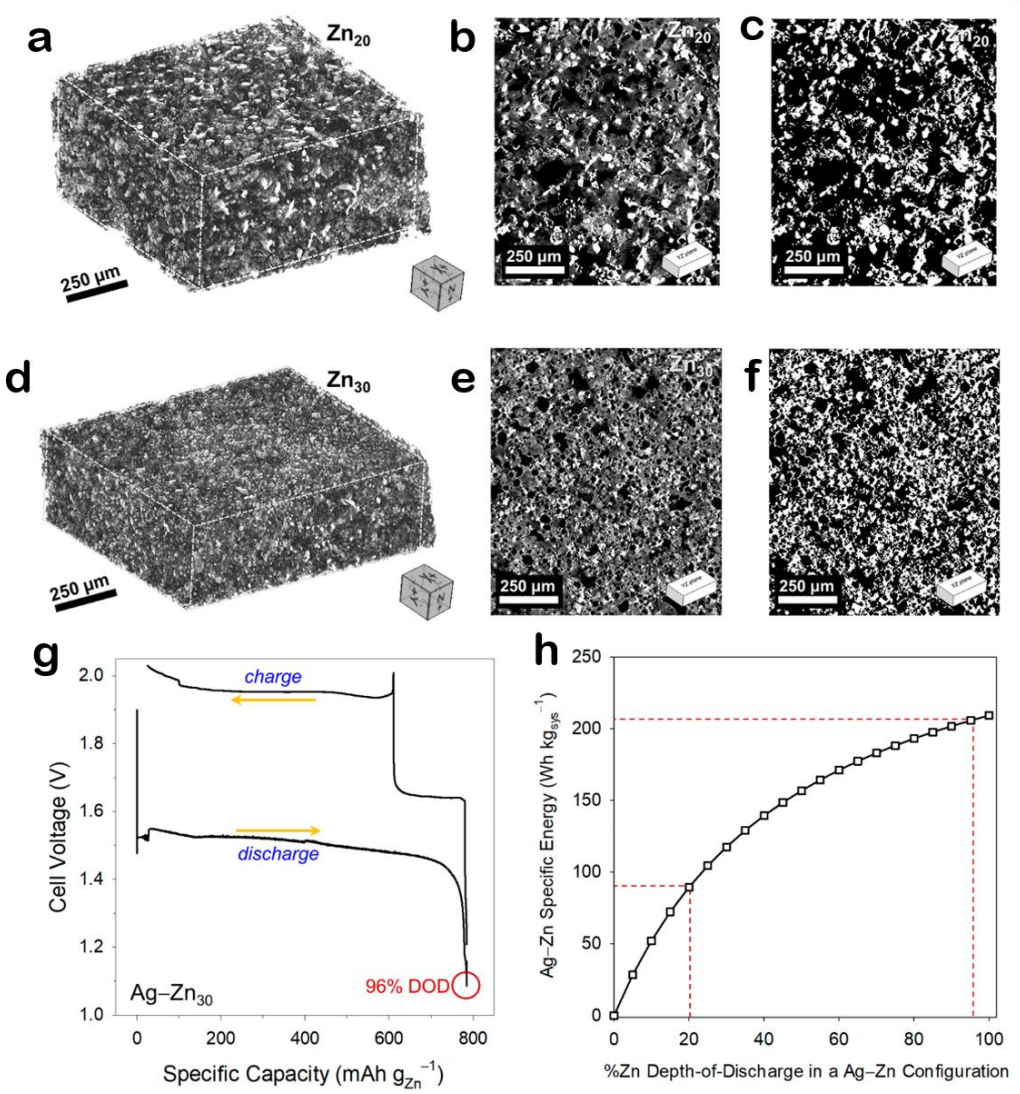

Fig. 7. 3D Zn sponges. 3D X-ray tomogram of (a-c) Zn_{20} and (d-e) Zn_{30} sponges. (g) Charge–discharge cycle at a C/15 rate for the Ag–Zn_{30} battery at near 100% utilization of Zn. (h) The calculated specific energy of a fully packaged Ag–Zn cell. Reprinted with copyright from Ref. [124].

Replacing Zn plate with the ZnO nanoparticles can buffer the volume change and suppress the dendrite growth as well [127]. Mcdevitt et al. created a spinodal-like microstructure by templating Zn precursors into self-assembled 13 (**Fig. 8**a and b) [128]. With the tailored design of the microstructures, the utilization efficiency of the ZnO anode almost reached 100%. Besides, the microstructural evolution and capacity loss in such

material was effectively suppressed and after 40 cycles, the electrode can still retain 90% of the first cycle capacity, while the one from powder dropped below 50% (**Fig. 8**c). The excellent performance is attributed to the continuity of fluid phases in the bijel template, which facilitate electric charge and ionic transportation.

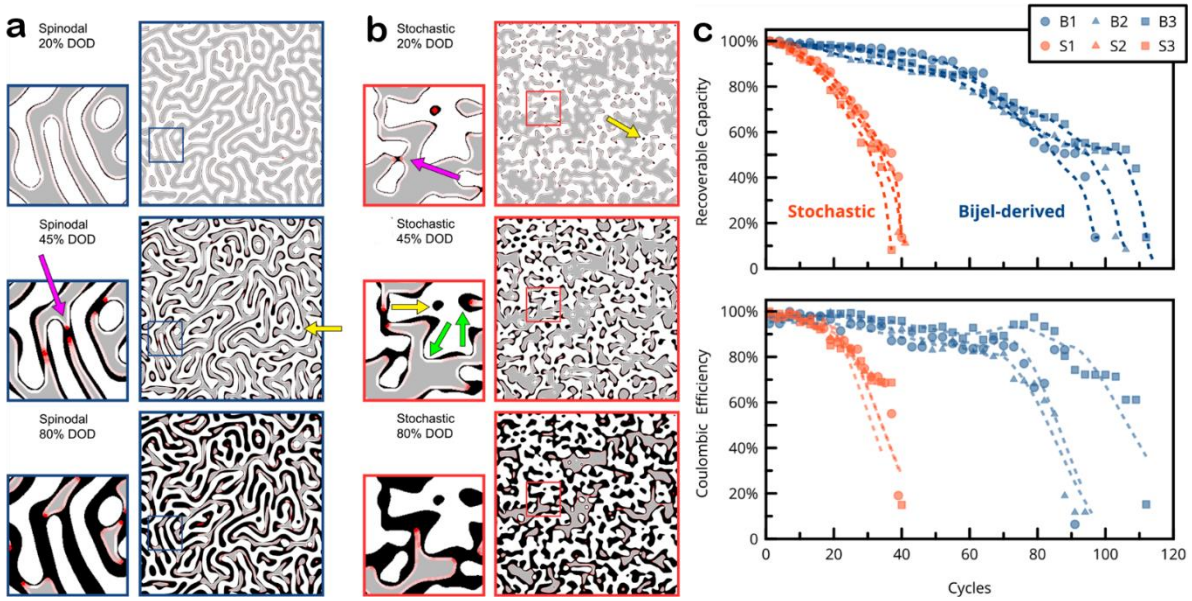

Fig. 8. Snapshots in the simulation for 20%, 45%, and 80% DOD for (a) the spinodal-like and (b) the stochastic structures. (c) Recoverable capacities (top) and Coulombic efficiencies (bottom) of stochastic and bijel-derived electrodes. Reprinted with copyright from Ref. [128].

The high capacity and energy density of Zn batteries is from the transportation of the two valence electrons. This also poses higher requirement on the cathode material for the storage of Zn^{2+} ions. To enable the fast intercalation of divalent Zn ions, electrode materials that are able to mitigate the electrostatic interaction between Zn ions and host crystal structure are very favourable.[117] Based on the extensive research, researchers have sorted out four types of electrode materials which might suit the application for Zn batteries, including the manganese and vanadium-based oxides, Prussian blue analogues and organic electrodes.

The report of $Zn_{0.25}V_2O_5 \cdot nH_2O$ has initiated extensive research over a wide range of vanadate materials, including $H_2V_3O_8$, LiV_3O_8, $Na_{0.25}V_2O_5$, $Na_2V_6O_{16}$, KV_3O_8, $K_{0.25}V_2O_5$, $K_2V_6O_{16}$, and $K_2V_8O_{21}$.[129-133] Besides of alkaline metals, calcium cations (Ca^{2+}) were also introduced into the vanadium oxides to form a $CaV_6O_{16} \cdot 3H_2O$ (CVO) cathode, which delivered a specific capacity of 252 mAh g^{-1} at 0.1 A g^{-1} [134]. La^{3+}, with a large atomic radius of 4.52 Å, was inserted in-between the VO layers and formed $LaVO_4$ with the interlamellar spacing increased from 11.9 to 13.7 Å [135]. A capacity of 472.5 mAh g^{-1} was achieved from the electrode at a current density of 0.38 A g^{-1}, and the ZIB as assembled delivered a peak energy density of 341.9 Wh kg^{-1}. Cations like NH_4^+ were also inserted into V_2O_5 ($(NH_4)_2V_{10}O_{25} \cdot 8H_2O$) [136]. Presence of NH_4^+ effectively enhanced the ionic conductivity of the Zn^{2+} and rearranged the structure of V_2O_5, leading to a high discharge capacity of 376 mAh g^{-1} at 0.5 A g^{-1} with a high energy density of 341 Wh kg^{-1}. For comparison, the electrochemical performances and variation in crystal structures of the V_2O_5 upon intercalation of different cations have been illustrated in **Fig. 9**. V_2O_5 doped with Ag can deliver a capacity around 215 mAh g^{-1}at 0.1 A g^{-1}, with an energy density of 118 Wh kg^{-1} at a power density of 0.136 kW kg^{-1} [137]. Insertion of cobalt ions increased the absorption energy of Zn^{2+} ions from 1.85 eV to 2.24 eV (**Fig. 10**), leading to a high intercalation/de-intercalation voltage of Zn^{2+} ions (1.7 V) and high energy density of 432 Wh kg^{-1} at 0.1 A g^{-1} [138]. Presence of oxygen vacancy could reduce the adsorption energy and diffusion barrier of the Zn^{2+} ions and the oxygen-deficient $K_2V_8O_{21}$ electrode delivered a high capacity of 385 mAh g^{-1} with excellent rate performance and stability [139]. Besides of intercalation of heteroatoms or metals, tailoring the microstructure of the V_2O_5 electrode is also effective.[45] For example, the porous V_2O_5 yolk-shell spheres exhibit a high capacity of 410 mA h g^- at 0.1 A g^{-1} [140].

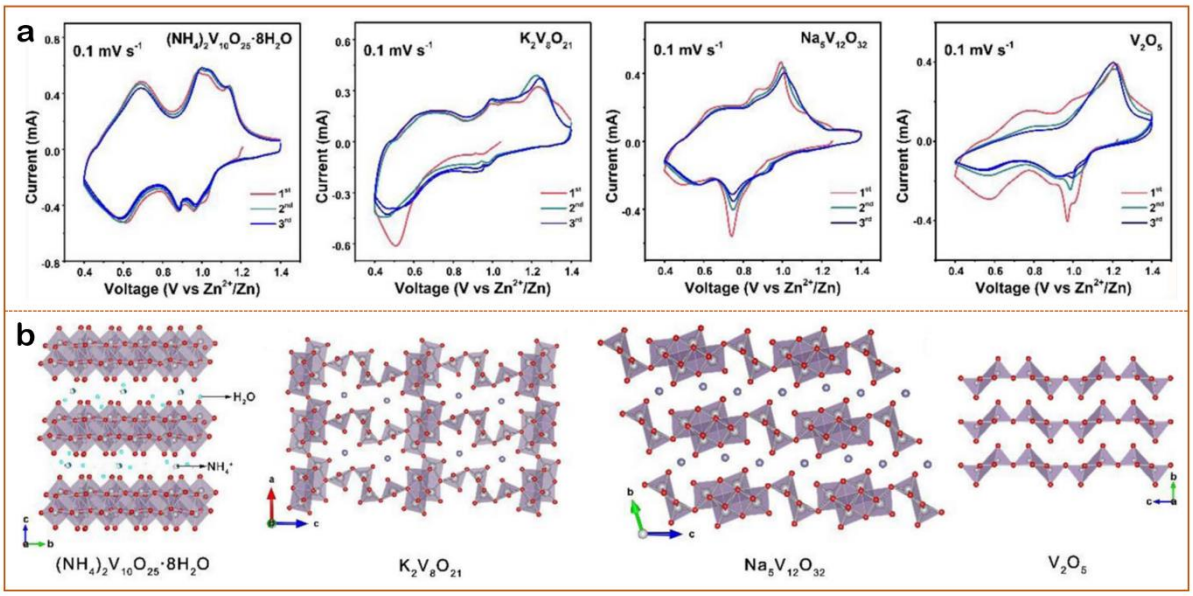

Fig. 9. Comparison of the V_2O_5 with presence of NH^{4+} and other cations. The CV curves (a) and the crystal structures (b) with intercalation of different cations. Reprinted with copyright from Ref. [136].

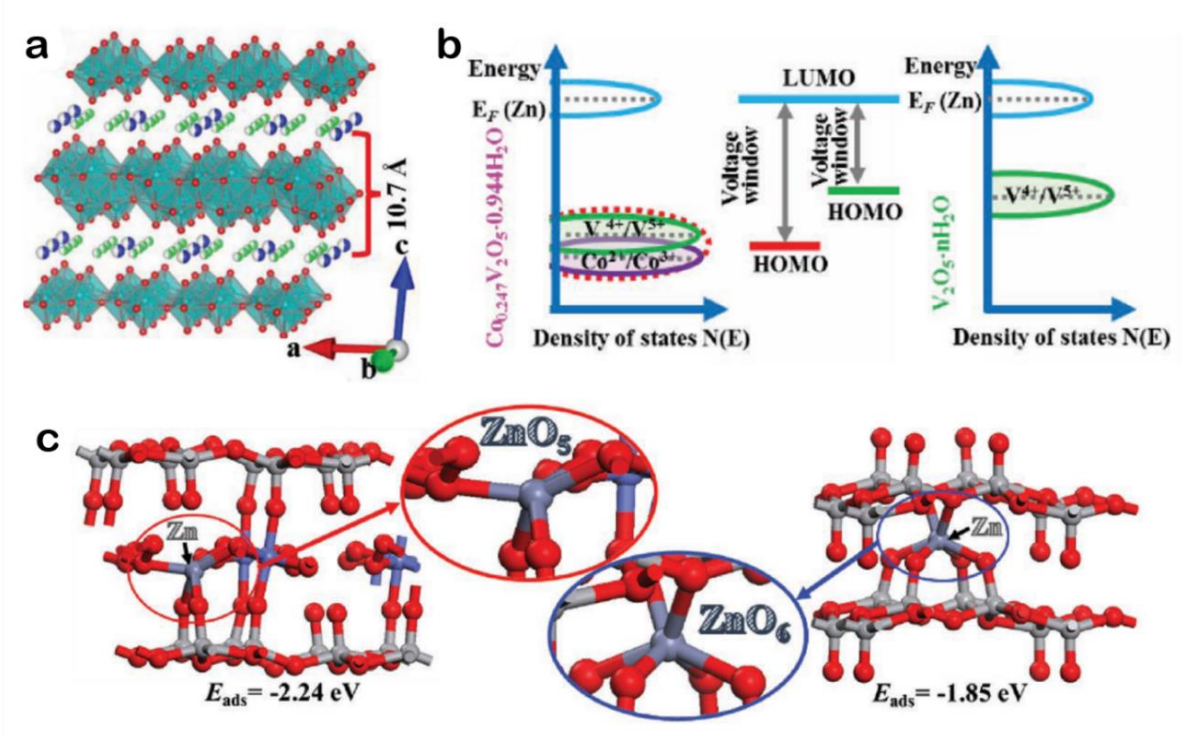

Fig. 10 (a) The crystal structure of $Co_{0.247}V_2O_5{\cdot}0.944H_2O$. (b) Schematic illustration of the energy versus DOS in $Co_{0.247}V_2O_5{\cdot}0.944H_2O$ and $V_2O_5{\cdot}nH_2O$ cathodes. (c) The optimized

configuration of Zn-adsorbed $Co_{0.247}V_2O_5 \cdot 0.944H_2O$ and $V_2O_5 \cdot nH_2O$ with the corresponding adsorption energies. Reprinted with copyright from Ref. [138].

Manganese-based cathodes, including $ZnMn_2O_4$, Mn_3O_4 and different polymorphs of MnO_2, including α-, β- and γ-MnO_2, are intriguing electrode materials for ARZBs. MnO were regarded as electrochemically inactive due to lacking tunnels to accommodate Zn ions. But they can become active cathode for Zn ion storage through an electrochemical activation process, by generating layered MnO_2 nanosheets around the MnO surface [141]. The cathode as-derived exhibited a high specific capacity of 330 mAh g^{-1} in $ZnSO_4$ aqueous electrolyte from the consecutive insertion of H^+ and Zn^{2+}. The interlayer spacing of manganese-based oxides could be further expanded by crystal water, which effectively shields the electrostatic interactions between Zn^{2+} and the oxide frameworks and promotes ion diffusion. The disadvantage of manganese-based electrodes is the dissolution of Mn into electrolyte and the drastic volume changes induced by the insertion of Zn ions or crystal water. To strengthen the structure, polyaniline was incorporated in between the layered MnO_2 to achieve a high capacity of 280 mAh g^{-1} with a high utilization efficiency (90%) [142]. The dissolution and slow kinetics of MnO_2 associated with their low electrical conductivity was effectively addressed by formation of $K_{0.8}Mn_8O_{16}$ (KMO) [143]. Presence of K^+ ions in the tunnel cavities stabilized the crystal structure and suppressed dissolution of MnO_2 (**Fig. 11**a), while introduction of oxygen vacancies accelerated the reaction kinetics (**Fig. 11**b). Benefit from the electrode optimization, the ARZB cell achieved a high energy density of 398 Wh kg^{-1} with long-term cyclability (**Fig. 11**c-d). Ren et al. fabricated few layer MnO_2 nanosheets with thickness around 1 nm from a template-directed synthetic procedure. These ultrathin MnO_2 nanosheets showed high surface area without stacking and aggregation and delivered a high capacity of 275.1 mAh g^{-1} at 0.3 A g^{-1} [144]. With the conversion reaction between Co(III)

rich-Co_3O_4 and CoO (Co(III) + $e^- \leftrightarrow$ Co(II) (1.83 V *vs. SHE*,)), the Zn/Co_3O_4 battery achieved a high voltage of 2.2 V in the mild aqueous electrolyte, which further led to a solid-state battery with a high energy density of 360. 8 Wh kg^{-1} [145].

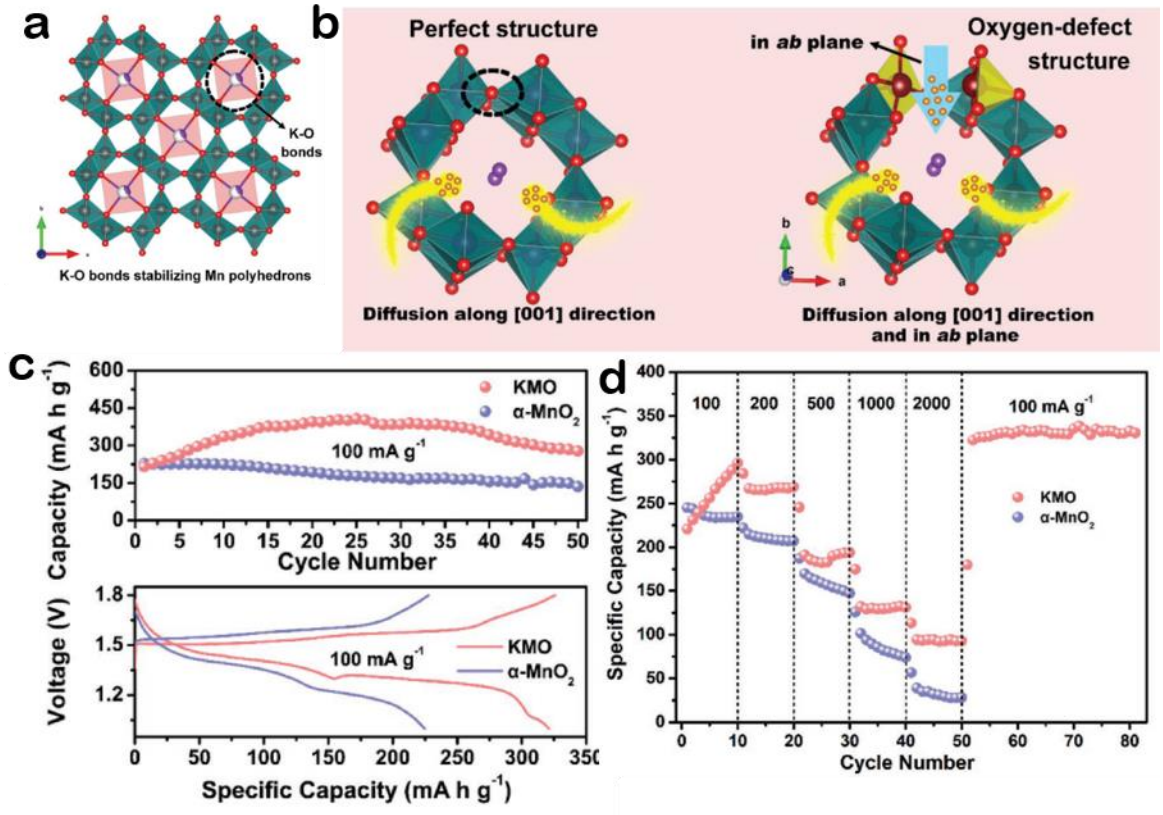

Fig. 11. (a) Illustration of the Mn polyhedrons with incorporation of K^+ ions. (b) H^+ diffusion into perfect and oxygen-defect KMO. The cycling, charge-discharge curves (c) and rate performance (d) of the KMO electrodes in comparison with the MnO_2 electrodes. Reprinted with copyright from Ref. [143].

Prussian blue analogues (PBAs) are also well-known electrode materials. Their open-framework structure enables facile insertion of metal ions and renders the electrodes superior rate performance. But so far, only limited work has investigated PBA electrodes for AZIBs probably due to their low capacity (< 60 mAh g^{-1}) and they are more susceptible to oxygen evolution reaction in aqueous electrolytes. With proper regulation over the structure and

composition, the performance can be improved. For example, with rhombohedral zinc hexacyanoferrate (ZnHCF) as cathode, which possesses large open sites in the porous 3D framework, a high voltage of 1.7 V with an exceptionally high energy density of 100 Wh kg^{-1} was achieved [11]. Copper hexacyanoferrate (CuHCF) was also investigated as cathodes for ZIBs in the aqueous solution of $ZnSO_4$ and the cell was able to deliver 90% of the theoretical capacity [146]. PBAs electrodes have also been integrated into hybrid battery systems and shown improved performance. For example, Hou et al. developed a hybrid Na/Zn battery with the stable electrochemical window up to 2.5 V with sodium manganese hexacyanoferrate $Na_2MnFe(CN)_6$ as cathode and sodium dodecyl sulphate (SDS) as electrolyte additives [4]. Wu et al. developed a reversible dual-ion battery based on the concentrated $ZnCl_2$ electrolyte (30 m) using a PBA cathode ($Zn_3[Fe(CN)_6]_2$) and the encapsulated ferrocene in microporous carbon as the anion-storage anode.[147]

Organic materials represent another intriguing type of electrodes for ARZBs. Quinone has proved to be able to promote the ion storage through coordinating with metal ions and oxygen atoms and achieve high energy densities [148]. The main concern of using organic electrodes is that they are prone to dissolve in the aqueous electrolyte and exhibit poor stability. Special separators are thus required to prevent the crossover of the soluble intermediates. Polymers are also expected to show less dissolution in the electrolyte with their covalently connected structure. Polydopamine (PDA) grafted onto carbon nanotubes delivered a capacity of 126.2 mAh g^{-1} from the redox reaction between catechol and ortho-quinone with adsorption and desorption of Zn^{2+} ions (**Fig. 12**a-c) [149]. Nam et al. introduced a redox-active triangular phenanthrenequinone-based macrocycle (PQ-Δ) featured with rigid geometry and layered superstructure (**Fig. 12**d-f) [150]. With co-insertion of Zn^{2+} and H_2O, the interfacial resistance between the cathode and electrolyte from decreased desolvation energy induced by the insertion of hydrated Zn^{2+} ions (**Fig. 12**g-h). A high reversible capacity

of 210 mAh g^{-1} was achieved from this electrode. Xia's group has identified an insoluble pyrene-4,5,9,10-tetraone (PTO) cathode, which delivered a high energy density of 186.7 Wh kg^{-1} by directly using glass fibres as the separator [151].

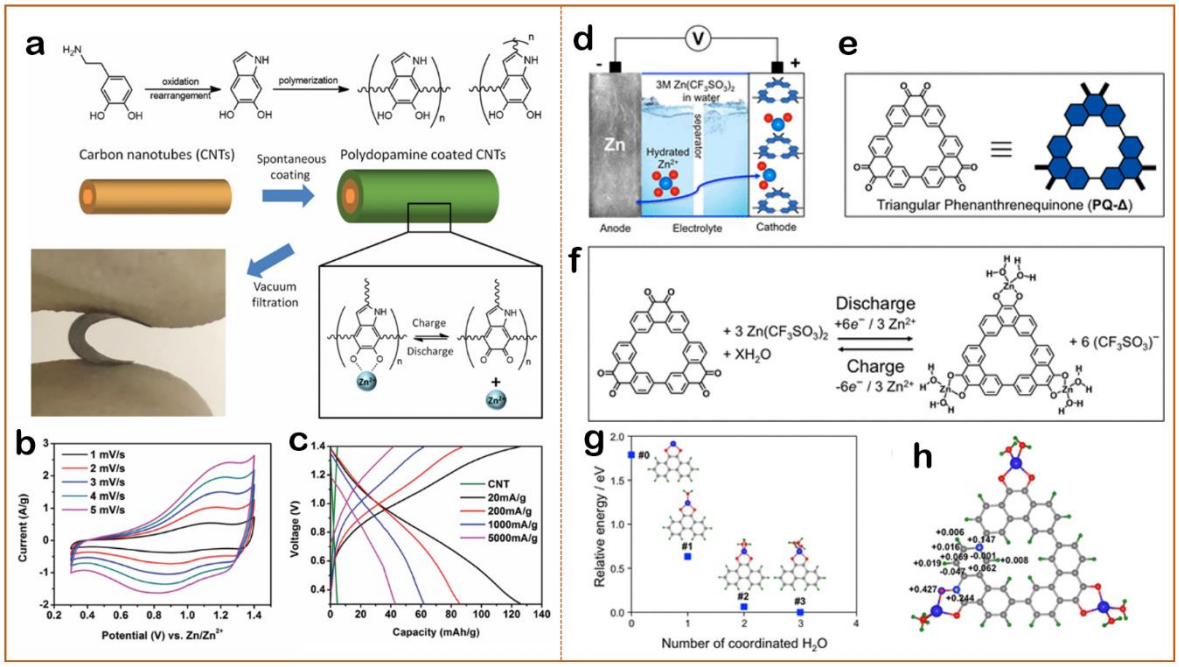

Fig. 12 (a) Illustration of the fabrication process and photo of the PDA grafted on carbon nanotubes. CV curves (b) and the charge-discharge profiles (c) of the PDA electrodes. Reprinted with copyright from Ref. [149]. (d) Schematic illustration of the aqueous rechargeable Zn/PQ-Δ cell. (e) Structural formula of PQ-Δ. (f) Electrochemical redox chemistry of PQ-Δ. (g) Relative energy values of Zn-coordinated PQ molecules. (h) Charge density increment for PQ-Δ after discharge. Reprinted with copyright from Ref. [150].

Because of the giant number of papers published, we summarized the electrode materials and their performance in recent two years in **Table 4** for a more straightforward comparison.

Table 4. Performance of ARZBs.

Cathodes	Electrolyte (solvent: water)	Operating Voltage (V)	Capacity (mAh g^{-1}@A g^{-1})	Energy density (Wh kg^{-1})	Ref
Porous V_2O_5 microspheres	2 M $Zn(CF_3SO_3)_2$	~0.7	401@0.1	286	[152]
$CaV_6O_{16}·3H_2O$	3 M $Zn(CF_3SO_3)_2$	~0.8	~325@0.05		[134]
Layer-expanded $V_2O_5·2.2H_2O$	3 M $Zn(CF_3SO_3)_2$	~1	450@0.1	324	[153]
Porous V_2O_5 nanofibers	3 M $Zn(CF_3SO_3)_2$	~1	319@0.02		[154]
VO_2 nanorods	1 M $ZnSO_4$	~0.7	353@1.0		[155]
Layered α -$Zn_2V_2O_7$ nanowires	1 M $ZnSO_4$	0.81	190.5@0.3	166	[156]
Ball-milled V_2O_5 powder	3 M $Zn(CF_3SO_3)_2$	~1	323@0.2	322	[157]
$Na_2V_6O_{16}·xH_2O$ with ample vacancies	1 M $ZnSO_4$	~0.8	~375@0.1	287	[158]
$Li_xV_2O_5·nH_2O$	2 M $ZnSO_4$	~1	470@0.5	423	[159]
$H_2V_3O_8$/graphene	3 M $Zn(CF_3SO_3)_2$	~0.8	394@0.1	168	[160]
$Na_{1.1}V_3O_{7.9}$ /graphene	1 M $Zn(CF_3SO_3)_2$	~0.7	191@0.05		[161]
$NH_4V_4O_{10}$	2 M $ZnSO_4$	~0.6	~425@0.3	374.3	[162]
$Na_{0.33}V_2O_5$	3 M $Zn(CF_3SO_3)_2$	~0.7	367.1@0.1		[163]
α-MnO_2/graphene scrolls	2 M $ZnSO_4$ + 0.2 M $MnSO_4$	~1.4	301.2@0.1	406.6	[164]
Polyaniline-intercalated MnO_2 nanolayers	2 M $ZnSO_4$ + 0.1 M $MnSO_4$	1.36	260@0.05		[142]
Ultrathin MnO_2 nanosheets	2 M $ZnSO_4$ + 0.5 M $MnSO_4$	~1.4	364@0.1		[126]
Pyrene-4,5,9,10-tetraone	2 M $ZnSO_4$	~1	336@0.04	186.7	[165]
Co(III) rich-Co_3O_4 nanorod@ carbon cloth	2 M $ZnSO_4$ + 0.2 M $CoSO_4$	2.2	205@0.5	360.8	[145]
VS_4@rGO	1 M $Zn(CF_3SO_3)_2$	0.73	250@0.2	180	[166]
Expanded MoS_2	1 M $ZnSO_4$	~0.6	202.6@0.1	148.2	[167]

Note: The energy densities are calculated based on the mass of cathodes.

2.5 Aqueous rechargeable magnesium batteries (ARMBs)

The first rechargeable Mg battery prototype was reported over 15 years ago and earlier rechargeable Mg batteries employed nonaqueous electrolyte system suffered from either low stability or high cost/hazard [168-170]. It was found by Sun et al. that water molecules presented in the MnO_2 lattice could facilitate the intercalation of Mg^{2+} ions, which has inspired a series of attempt in achieving aqueous rechargeable magnesium batteries (ARMBs) [171]. The charm of aqueous Mg batteries lies in the high volumetric specific capacity (3833 mAh L^{-1}) and absence of dendrite formation on the metal Mg. It means potentially metal Mg can be directly used as the anode, which guarantees the battery system with high energy densities and lower cost. Because of the detrimental formation of dendrites deposited on metal Li, the current LIBs have to employ graphite as the anode material and sacrifice a great extent of the capacity density (from 2046 mAh L^{-1} to 850 mAh L^{-1}).[171] Besides, Mg is cheaper and safer, i.e., metal Mg can be handled in ambient atmosphere in contrary to the strict and expensive apparatus required for the reactive metal Li. However, Mg is prone to severe corrosion in aqueous electrolytes, resulting in low utilization efficiency of the anode (~60%), which hampers the specific energy density of the aqueous Mg battery.[172-174] The corrosion and dissolution of the Mg anode would also aggravate the hydrogen evolution with the negative difference effect (NDE) and reduce the current efficiency in aqueous electrolytes. To alleviate the self-corrosion and improve utilization efficiency of the Mg anode, one effective strategy is to alloy Mg with different metal species, such as Al, Pb, Hg, Li and Sn.[175-178] Trace amount of Li could enhance discharge activity of the Mg anode. Addition of minor amount of rare earth element, like Ce and Y, further improves the performance of the alloyed Mg-Li anodes.[179] Alloying with Sn could reduce the self-discharge of pure Mg and form a passive film on the anode surface.[180] Mg-Ca and Mg-Fe systems have been theoretically investigated to study their effect on the stability of the Mg anode surface and

presence of Ca and Fe could alter the electrochemical reactions on Mg (001) surface.[181] Despite the anode efficiency has been improved, some fundamental issues are still under debate in the understanding of the dissolution/corrosion of the Mg anode. Because of the existing issues of the Mg anodes, three-electrode systems or more stable graphite anode are often employed when people investigate performance of electrode materials for aqueous Mg batteries. Cao's group have developed the $FeVO_4$ anode and coupled it with the Mg-OMS-1 (OMS=octahedral molecular sieves) cathode [182, 183]. The $FeVO_4$ with tailored porous structure has delivered a high energy density of 70.4 Wh kg^{-1}.

On the other hand, suitable cathode materials with high operation voltage and excellent Mg storage capacity is also of great significance to achieve high-energy aqueous Mg batteries. Wang et al. have employed $Li_3V_2(PO_4)_3$ and poly pyromellitic dianhydride as the Mg ion host materials, and in combination with a highly concentrated $Mg(TFSI)_2$ (4 m, mol/kg) electrolyte, the full cell has delivered a high operating voltage of 1.9 V and a high energy density of 62.4 Wh kg^{-1} [184]. The enhanced performance is originated from the H_2O presented in aqueous electrolyte, which improves mobility of Mg^{2+} ions and shields the multi-charge effect of the Mg^{2+} ions. The high concentration of Mg-containing electrolyte also favours the reversible Mg^{2+} insertion/extraction in the host structure. Chen et al. coupled the nickel hexacyanoferrate (PBN) with an aromatic polyimide anode and the aqueous Mg ion full cell delivered a reversible capacity of 33 mAh g^{-1} with a maximum operational voltage around 1.5 V, corresponding to an energy density of 33 Wh kg^{-1} [185]. Manganese oxides are also promising host materials for the Mg^{2+} ions [186]. Cabana et al. have reported their capability in achieving high-voltage Mg intercalation at a voltage of ~2.9 V (vs. $Mg^{2+/}Mg$) [187]. Later, Tao et al. have fabricated 3D hollow spheres of the $MgMn_2O_4$ and investigated their electrochemical performance as cathode for aqueous Mg ion battery [188]. It was revealed that the Mg^{2+} ions can be reversibly intercalated into the tetragonal-spinel structure

and realized a high operation plateau of 3.2 V (vs. Mg^{2+}/Mg) and a reversible capacity of 261.5 mAh g^{-1}. One major consideration in the design of electrode materials is to address the strong electrostatic interaction and poor dynamics in the intercalation of the divalent Mg^{2+}. It has been massively reported that the crystal water can effectively shield the electrostatic interaction between the guest multivalent ions and host crystal structure. Ni-based layered structure bearing the active redox centre of Ni^{2+}/Ni^{4+} with crystal water worked as a stable host structure [189]. The system delivered a high capacity of 190 mAh g^{-1} at 3.1 V (vs. Mg/Mg^{2+}), corresponding to an exceptionally high capacity of 589 Wh kg^{-1}.

Performance of the ARMBs with the properties of electrode materials and electrolytes have been summarized in **Table 5**.

Table 5. Performance of the ARMBs.

Cell type	Electrolyte (solvent: water)	Operating Voltage (V)	Capacity (mAh g^{-1}@A g^{-1})	Energy density (Wh kg^{-1})	Ref
Cathode: $Li_3V_2(PO_4)_3$@C Anode: Poly pyromellitic dianhydride	4 m $Mg(TFSI)_2$	1.9	52@0.1	62.4	[184]
Cathode: $Na_{1.4}Cu_{1.3}Fe(CN)_6 \cdot 5H_2O$ Anode: Polyimide	1 M $MgSO_4$	1.3	~35@0.5	45	[185]
Cathode: $Mg_{1.1}Mn_6O_{12} \cdot 4.5H_2O$ Anode: Graphite rod	0.2 M $Mg(NO_3)_2$	~0.1 (vs. SCE)	250@0.01		[190]
Cathode: Mg-OMS-2/graphene Anode: Activated carbon	0.5 M $Mg(NO_3)_2$	0 (vs. SCE)	44.1@0.1	46.9	[191]
Cathode: $MgMn_2O_4$/rGO Anode: Graphite rod	0.5 M $MgCl_2$	~0.3 (vs. SCE)	140.1@1.0		[192]
Cathode: Mg-OMS-1 Anode: $FeVO_4 \cdot 0.9H_2O$/graphene	1 M $MgSO_4$	1.8	65.1@0.05	58.5	[183]
Cathode: Mg-OMS-1 Anode: Porous $FeVO_4$/C	1 M $MgSO_4$	1.8	58.9@0.1	70.4	[182]
Cathode: α-MnO_2/CNT Anode: Pt	1 M $MgSO_4$	~0.25 (vs. SCE)	144.6@0.5		[193]
Cathode: MgOMS-1/graphene Anode: Carbon molecular sieve	0.5 M $Mg(NO_3)_2$		64.8@0.1		[194]
Cathode: Mn_3O_4 Anode: Activated carbon	2 M $MgSO_4$	2	81@0.5	20.2	[195]
Cathode: Mg-OMS-7 Anode: Graphite rod	0.2 M $Mg(NO_3)_2$	~0.2 (vs. SCE)	283.1@0.01		[196]
Cathode: $LiFePO_4$/C Anode: Pt	1 M $MgSO_4$	~0 (vs AgCl/Ag)	82@0.017		[197]
Cathode: $Li_xNi_{0.5}Co_{0.2}Mn_{0.3}O_2$ Anode: Pt coil	1 M $MgSO_4$	~3	190@0.02	589	[189]

Cathode: $MgMn_2O_4$ Anode: Pt	1 M $MgSO_4$	3.2	261.5@0.1		[188]
Cathode: $MgFe_{1.33}Mn_{0.67}O_4$ Anode: Graphite rod	0.5 M $MgCl_2$	~0.2 (vs. SCE)	136.5@0.05	369.6	[198]

2.6 Aqueous rechargeable aluminium batteries

Aluminium (Al) is a naturally abundant, trivalent charge carrier with extremely high volumetric capacity (8040 mAh cm^{-3}).[199] However, most Al cells, including Al-air and Al-S batteries could not be recharged in aqueous media. This is because the standard potential of Al^{3+}/Al (-1.68 V) is lower than H^+/H_2, and the evolution of H_2 occurs due to the reaction between Al foil and the aqueous solution. The formation of a high-bandgap passivating oxide coating makes Al electrochemically inert and high potentials are thus required to drive ion transportation through the passivation layer, which easily exceeds the thermodynamic stability limits for water, resulting in continuous electrolyte degradation and hydrogen generation during the battery recharge. It was later found that electrolytes based on the acidic ionic liquid (IL) melt aluminium chloride ($AlCl_3$)-1-ethyl-3-methylimidazolium chloride ([EMIm]Cl) could overcome oxide passivation and enable rechargeable Al battery [200]. This has initiated several research works by mildly corroding the Al surface to activate the Al striping and plating reaction [201-204]. Zhao et al. tried to combine the merits of both IL and aqueous electrolyte [205]. They tried to generate a tight IL-enriched film on the interface that protects the Al surface from formation of metal oxide. The treated electrode exhibited exceptional reversibility in both symmetric Al cells and full cells, e.g., a high specific energy of 500 Wh kg^{-1} (based on the MnO_2 mass in the cathode) was achieved. He et al. made a further modification over the electrolyte with pre-addition of $MnSO_4$ into the aqueous aluminium trifluoromethanesulfonate ($Al(OTF)_3$) solution [206]. In this strategy, Birnessite MnO_2 was used as the cathode and Al foil anode was treated with IL ($AlCl_3$/[EMIm]Cl) (**Fig.**

13a). With pre-addition of $MnSO_4$, the stability and rate capability of the battery was improved (**Fig. 13**b-d). The cell achieved a high energy density of 620 Wh kg^{-1} (based on the MnO_2 mass) and a high discharge voltage of 1.35 V. After cycling for 65 times, it still maintained a capacity of 320 mAh g^{-1}. And the mechanism study revealed that Birnessite MnO_2 cathode dissolved in the electrolyte in the initial discharge process, and in the later cycles re-formed into a non-crystallized $Al_xMn_{1-x}O_2$ compound which enabled the reversible charge/discharge of the battery, i.e., both Al^{3+} and Mn^{2+} was involved as the charge carriers. Joseph et al. further introduced some guest K^+ ions into MnO_2 structure to provide extra space for the intercalation/de-intercalation of Al^{3+} ions (**Fig. 13**e and f). But the specific capacity of the modified electrode is moderate with around 109 mAh g^{-1} [207]. Despite treatment of the Al with the chloroaluminate-based ionic liquid electrolytes is effective, this strategy cannot eliminate the usage of corrosive and H_2O/air-sensitive ionic liquid, thereby still posing challenges in the handling and testing of the battery and incur certain safety issues. Nandi et al. explored an Al-metal battery without pre-treatment of the Al metal with ionic liquid [208]. Instead, they electrochemically pre-treat the Al foil in 1 M $AlCl_3$ aqueous electrolyte, and the presence of Cl^- could eliminate the Al_2O_3 on the Al surface and improve its electrochemical activity. Such Al-metal battery delivered an initial capacity of 213 mAh g^{-1}, but it dropped to 88 mAh g^{-1} after 50 cycles because of severe corrosion of Al metals upon reaction. Therefore, it would require replacement of fresh Al anode to realize rechargeable Al-metal battery. As demonstrated by Zheng et al., the deposition behaviour of Al can be also effectively regulated with formation of evenly distributed and nanosized electrodeposits on the (111)–textured gold (Au) nanosheets [123].

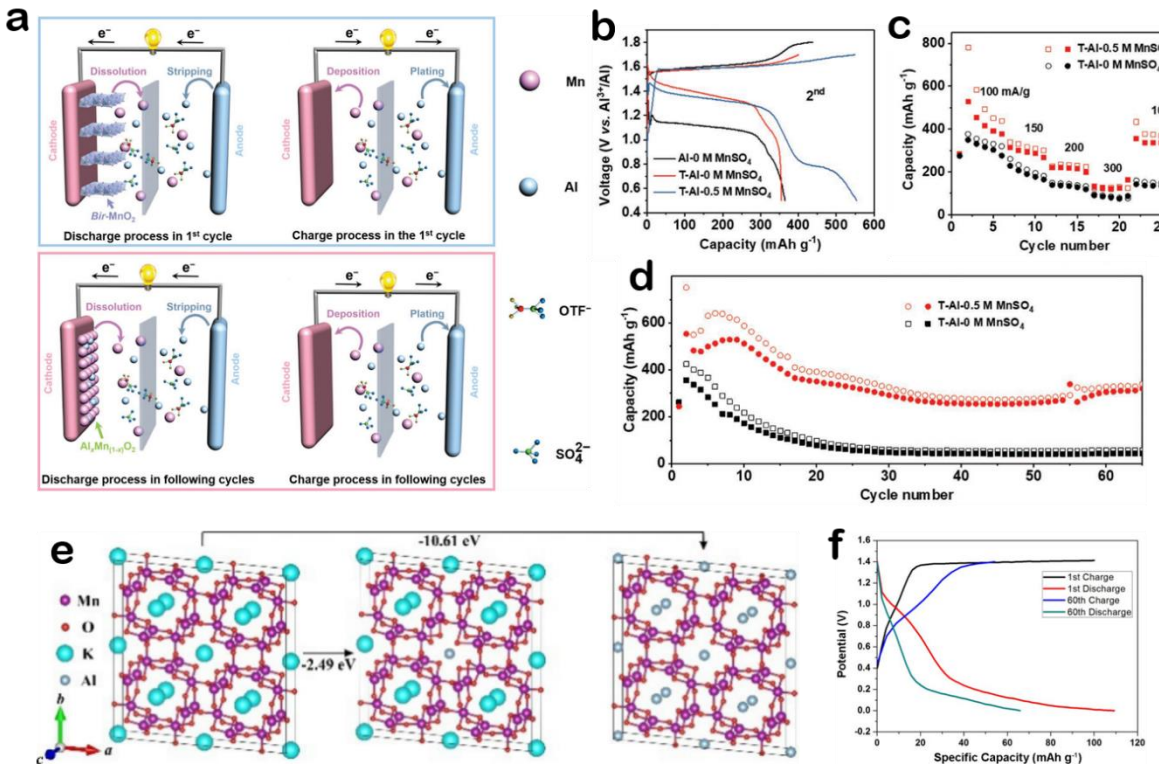

Fig. 13. (a) Illustration of the charge-discharge process of the Al-MnO_2 battery in the 1st and subsequent cycles. (b) Charge-discharge curve, (c) rate performance and (d) cycling stability of the battery with/without $MnSO_4$. Reprinted with permission from Ref. [206]. (e) Scheme illustration of the intercalation of Al^{3+} into the K-rich cryptomelane structure. (f) Comparison of the 1st and 60th charge-discharge profiles of cryptomelane. Reprinted with permission from Ref. [207].

The strong electrostatic nature of Al^{3+} leads to sluggish kinetics, high over-potentials, and eventual collapse of the host structure, which represents one grand bottleneck for the development of Al ion battery. The weak bond strengths between the host frameworks (namely, moderate polarity) are preferable in an ideal cathode for Al-based battery. Sulfur (S), transition metal sulphides, Prussian blue analogues (PBAs) and some transition metal oxide (MO_x, M= V or Ti) can meet this requirement [209, 210]. They can promote reversible trivalent reaction. However, their discharge voltage is relatively low and only ranged from

0.3 to 0.8 V. Carbon based material with high surface area such as 3D graphite foam have enabled ultrafast monovalent reaction kinetics and delivered high power density, but the monovalent reaction limits the specific capacity [211]. The other type of cathode, such as S, SnS_2 [212], Ni_3S_2 [213], V_2O_5 [214], CuS [215] and NiS [216] can potentially realize trivalent reaction and achieve high specific capacity, however, most of reported result were from ionic liquid. Wu et al. synthesized $Al_xMnO_2{\cdot}nH_2O$ by in-situ electrochemical transformation from the spinel to layered transformation of the Mn_3O_4 precursor (**Fig. 14**a) [217]. The $Al_xMnO_2{\cdot}nH_2O$ cathode has outperformed its precursor Mn_3O_4, with an initial capacity as high as 467 mAh g^{-1} and a high voltage of 1.2 V (**Fig. 14**b). With the configuration of Al/Al(OTF)s-H_2O/$Al_xMnO_2{\cdot}nH_2O$, the cell achieved a high energy density of 481 Wh kg^{-1}. In contrary to the Birnessite phase formed upon transformation from other metal ion batteries, e.g., Li^+ and Na^+, the intercalation of trivalent Al^{3+} ions has resulted in an amorphous structure with layered phase (**Fig. 14**c). Such layered structure benefited the insertion of Al^{3+} ions and the crystal water presented further helped to shield the electrostatic interaction of Al^{3+} with the host material. Therefore, the stability and reaction kinetics of the battery were significantly improved (**Fig. 14**d-e). For the Al ion battery, an aqueous electrolyte system might be more beneficiary rather than the commonly adopted IL system. Since the IL is “dry” and hydrophobic and cannot realize the water-assisted reaction process. Now, more research efforts are devoted to the study of the aqueous rechargeable Al ion battery, or other multivalent ion batteries [218].

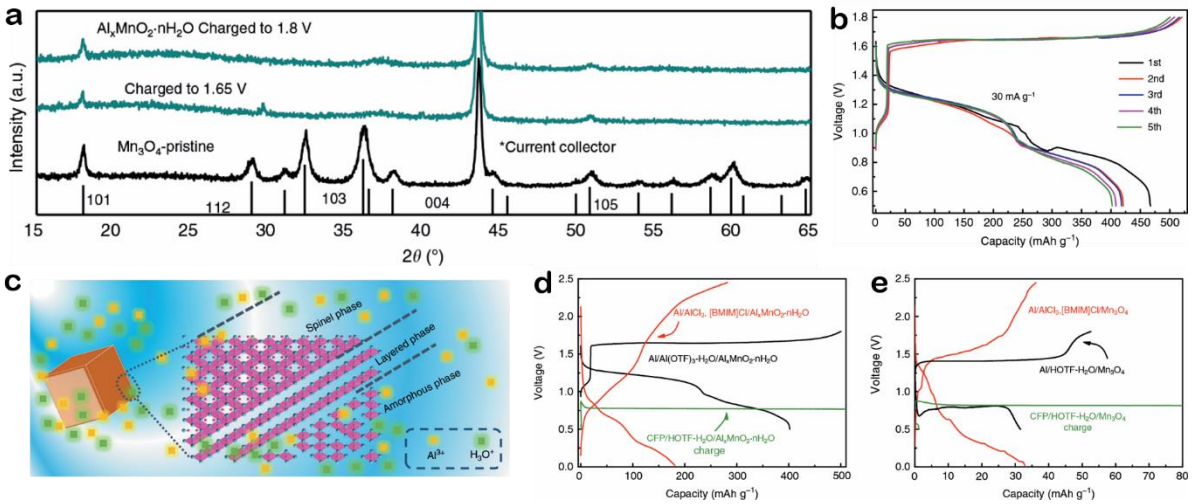

Fig. 14. (a) XRD patterns of Mn_3O_4 and $Al_xMnO_2{\cdot}nH_2O$. (b) Charge-discharge curve of the battery consisted of $Al/Al(OTF)_3$-$H_2O/Al_xMnO_2{\cdot}nH_2O$. (c) Illustration of $Al_xMnO_2{\cdot}nH_2O$ with mixed phases. (d-e) Typical charge-discharge curves of different batteries. Reprinted with permission from Ref. [217].

For the Al ion batteries, the energy output is often expected to be realized through the migration of the Al^{3+} ions, as in the case of LIBs. However, doubts have been raised from the tiny capacities as obtained. Kim et al. thus carried out a fundamental study to elucidate the charge storage mechanism by using TiO_2 as the model electrode. It is revealed that the charge carrier in the aqueous electrolyte is proton, donated by the hexagonal complex $[Al(H_2O)_6]^{3+}$, rather than the commonly assumed multivalent ions, e.g., Al^{3+}, Mg^{2+} and Zn^{2+} [219]. This research has offered a new direction in understanding the charge-storage mechanism of multivalent ion batteries. For now, it is still hard to draw a conclusion from the existing results. For some people, intercalation of Al^{3+} in the metal oxide lattice are challenging because the strong Coulombic interactions will impede solid state diffusion. While evidences have shown that the presence of crystal water could shield such electrostatic interaction and the insertion of Al^{3+} ions or co-insertion of both Al^{3+} ions and proton, cannot be completely ruled out.

Electrode materials, electrolytes used and the performance of the as-assembled ARABs have been summarized in **Table 6**.

Table 6. Property and performance of the ARABs.

Cell type	Electrolyte	Voltage (V)	Capacity (mAh g^{-1}@A g^{-1})	Energy density (Wh kg^{-1})	Ref.
Cathode: $K_{0.2}Fe[Fe(CN)_6]_{0.79}\cdot 2.1H_2O$ Anode: Activated carbon	5 M $Al(CF_3SO_3)_3$	~0.25 (vs Ag/AgCl)	116@0.15		[220]
Cathode: Cryptomelane MnO_2 Anode: Pyrolytic graphite	1 M $Al(NO_3)_3$	~0.8	109@0.02	33.29	[207]
Cathode: Bi_2O_3 Anode: Al	1 M $AlCl_3$	0.55	103@1.5		[221]
Cathode: Copper hexacyanoferrate Anode: Polypyrrole coated MoO_3	1 M $Al(NO_3)_3$	~0.6	31@0.2		[222]
Cathode: $Al_{0.25}Na_{0.81}V_2(PO_4)_2$	0.1 M $AlCl_3$	~0.4 (vs Ag/AgCl)	~105@0.06		[223]
Cathode: V_2O_5 Anode: Al	2 M $Al(OTF)_3$	0.9	186@0.04		[224]
Cathode: Graphite PMMA Anode: Al	49 m $AlCl_3\cdot 6H_2O$	1.85	165@0.5	220	[225]
Cathode: $Al_xMnO_2\cdot nH_2O$ Anode: Al	5 M $Al(OTF)_3$	~1.1	467@ 0.03	481	[226]
Cathode: MoO_3	0.5 M $Al_2(SO_4)_3$	-0.3 (vs Ag/AgCl)	~800@2.5		[227]
Cathode: $FeVO_4$ Anode: Al	1 M $AlCl_3$	-0.2 (vs Ag/AgCl)	~350@0.06		[228]
Cathode: α-MnO_2 Anode: Al	2 M $Al(CF_3SO_3)_3$	~1.3	~380@0.1	~500	[205]
Cathode: TiO_2/CNT	1 M $AlCl_3$	~1	225.5@0.05		[229]
Cathode: $K_2CoFe(CN)_6$	1 M $Al(NO_3)_3$	~0.5 (vs Hg/Hg_2Cl_2)	50@0.1		[230]
Cathode: WO_3	1 M $AlCl_3$	-0.4 (vs Ag/AgCl)	~140@2.5		[231]

3. Conclusion and future perspectives.

The current market is still dominated by LIBs with organic electrolyte. With their foreseeable market share in consumer electronics and the transport section, the potential safety hazards associated with usage of the flammable organic solvents have become more pronounced issues. The academic community has devoted extensive efforts to the

development of alternative battery technologies with better safety and lower cost. Aqueous metal ion batteries are among the most promising candidates.

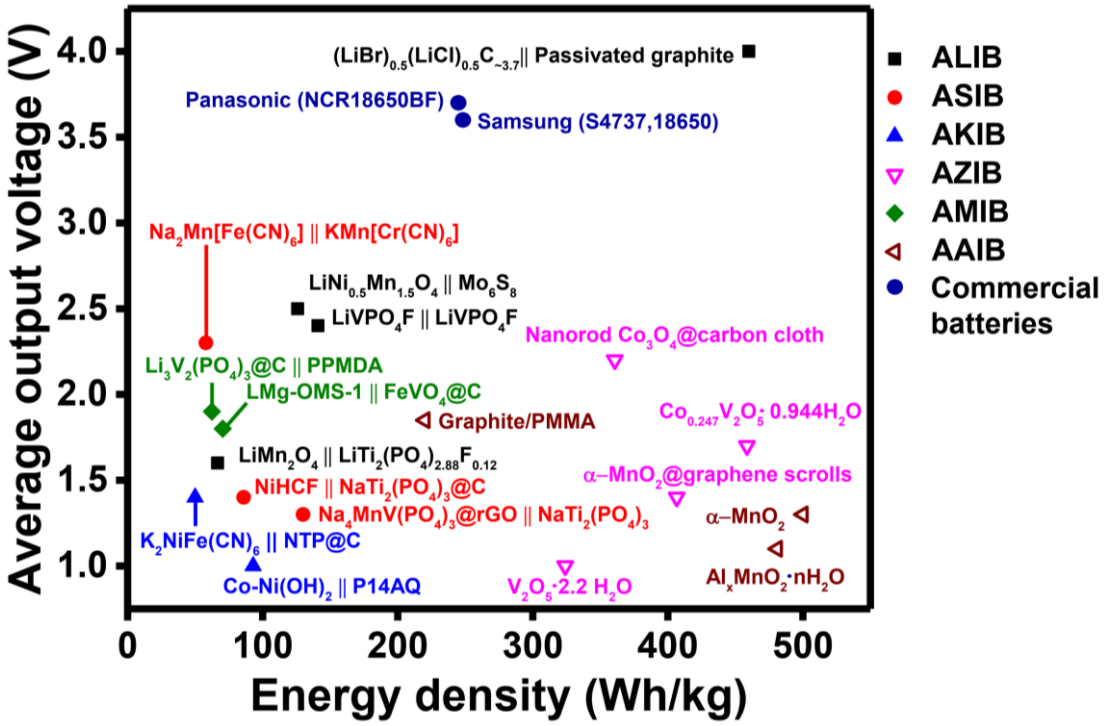

Fig. 15. Diagram illustrates the representative energy densities and voltage output of different aqueous rechargeable batteries (energy densities of AZIBs and AAIBs are determined by the mass of the cathode material, and others are based on the total mass of the cathode and anode).

Despite of the intriguing potentials, the current aqueous metal batteries are still facing many challenges associated with the low voltage of electrolyte, low capacity and dissolution of electrode materials, undesirable side reactions on the metal anode, etc. The extensive research efforts in recent years have brought about significant breakthrough in the energy density in the aqueous metal batteries (**Fig. 15 and 16**). At the meantime, practice of the new concept of "dual ion batteries" and "conversion-intercalation" chemistry has further opened new pathways to further increase capacity of traditional electrode materials. The concept of combining both catalysis and aqueous battery have been employed in the construction of the

Zn–Mn hybrid aqueous battery with intriguingly high energy density [232-233]. It is worth of future exploration of this strategy in expanding the voltage window and improving the overall performance of the aqueous battery system. Machine learning represents another appealing direction in determining the charge status and health status of the battery. By incorporating materials information into a new explainable model and performing in situ calculations, machine learning techniques can accurately predict the length and time of the battery, which is of great significance of their widespread applications in EVs. [234]

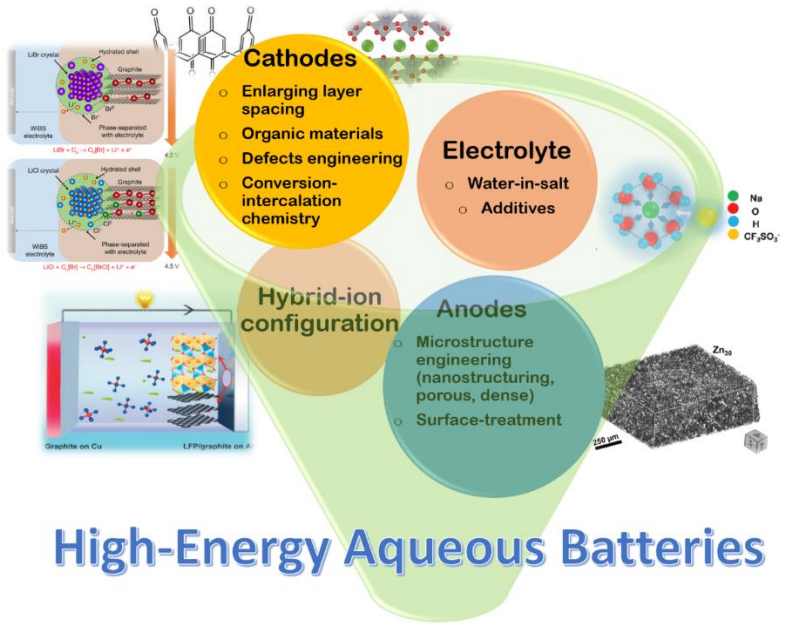

Fig. 16. Typical strategies developed to achieve high-energy aqueous rechargeable batteries.

In the future, the energy density of rechargeable aqueous metal ion batteries can be improved from the following aspects.

3.1 Regulating the anodes and electrolyte interfaces

The dissolution and corrosion of metal anodes in water hampers the long-term stability of the aqueous metal batteries. For the active metals such as Li, Na and K, surface coating or

forming an artificial SEI layer similar with that formed in the organic electrolyte has proved to be efficient strategy to enable their direct application in the aqueous electrolyte. But the composition of such artificial SEI layer is very complicated. Employment of more advanced characterization technology to analyse the composition or visualize the evolution of the SEI layer in the cycling process would be very helpful. Besides, it was expected that the more stable metals such as Zn, Mg and Al can be directly applied as anodes. But issues like dendrite growth, corrosion, and undesired side reactions have emerged in the aqueous electrolytes and severely affected the stability and safety of the batteries. In the future, increasing their electrochemical activity and engineering their microstructure to further improve the anode utilization efficiency would be highly necessary. Besides, suppress the dendrite growth and eliminate the undesirable side reactions on these metal surfaces with effective coating ensures the long-term cycling and safe operation of the batteries.

3.2 Microstructure engineering and suppressing dissolution of the cathode materials.

When selecting cathode materials for aqueous batteries, the redox potential should be put into first consideration. Only materials with the voltage within the water decomposition window can be used. But the redox potential of electrode materials is also affected by the pH value, concentration of electrolyte and crystal orientations. When exploring novel cathode materials for the aqueous system (especially in the concentrated electrolytes), all the above parameters need to be carefully re-evaluated. Besides, other than voltage, the specific capacity of materials also determines the energy density of the battery. Introduction of the redox couples (Ni^{2+}/Ni^{4+}, Mn^{2+}/Mn^{4+}) could significantly improve the specific capacity.

On the other hand, the dissolution of cathode materials, particularly Mn-containing cathodes, should be addressed to avoid the capacity decay. With additives like $MnSO_4$ in the

electrolyte, the dissolution can be mitigated. However, the long-term effect of these additives on the battery performance needs to be evaluated. Surface coating on the electrodes surface can act as a protective layer and prevent their dissolution. But the electrochemical activity and weight ratio of the coating layer also affects the overall energy density of the battery. Moreover, doping with certain cations (such as Ti^{4+}, Al^{3+}) into the crystal structure could effectively suppress the dissolution of Mn species into the aqueous electrolyte. Further efforts are still required on the selection of the dopants and development of more effective doping strategies.

Batteries based on multivalent ion storage (Zn^{2+}, Mg^{2+}, Al^{3+}) have been extensively explored over the recent years. Selection of cathode materials with both fast redox kinetics and fast transportation of the multivalent ions is extremely challenging because of the larger ionic sizes and the much stronger electrostatic interactions with the host structures. To shield the electrostatic interactions and stabilize the crystal structure for multi-valent ion storage, the presence of crystal water in the electrode structure has proved to be imperative. Better understanding of water-containing electrode materials and their interaction mechanism with the aqueous electrolyte can lead to more rational and target-driven design of the aqueous battery systems. Moreover, even potentially the multi-electron transfer process will bring about larger specific capacity, the voltage of most metal ion batteries still can not compete with the Li ion battery. And it has been observed that in contrary to the flat and stable plateau presented in the Li and Na ion batteries, the discharge profile of the multivalent ion batteries rarely shows stable plateau. This will affect the energy density and voltage output the battery for practical application. More fundamental understanding about the unstable voltage issues should be elaborated.

Organic electrode materials that can promote multi-electron transfer process are another popular option. The main challenge is their moderate reversibility, low output voltage, and

large polarization when reacting with multivalent metal ions. Their dissolution in diluted aqueous electrolytes is also a nonnegligible issue. With the concentrated electrolyte, the dissolution can be greatly reduced. Besides, with optimization of molecular weight and polymerization degree, the energy density of organic electrode materials can be further improved. However, the specific capacity and stability must be balanced with proper polymerization degree. On the other hand, exploitation of more feasible organic materials and in-depth mechanistic understanding of these organic molecules with the electrolyte and metal ions would also be helpful to push forward their further commercialization.

3.3 Exploration of water-in-salt electrolyte with lower cost

Electrolyte system of aqueous metal ion batteries has been improved through pre-addition of certain additives or surfactants which can effectively suppress the dissolution of electrodes and slightly widen the operating voltage window. However, it is the introduction of the "water-in-salt" concept that revolutionarily addressed the low-voltage issue in the aqueous system. The voltage of the aqueous battery system can now be pushed up to 4 V with the highly concentrated electrolytes of different compositions. Besides, with the application of the "water-in-salt" electrolyte, the parasitic side reactions related with decomposition of water, such as hydrogen evolution reactions, can be effectively suppressed. From the safety point of view, this has made the assembly of the full cells based on the "water-in-salt" electrolyte more feasible. But several challenges need to be addressed before their further commercialization. First, the highly concentrated electrolyte tends to crystallize at room temperature or below and may bring about instability in the battery performance. Precipitation of concentrated Li salts brings about safety concerns.[32] In this case, the composition and structure of the electrolyte needs to be further optimized to enable them for wide-temperature applications. On the other hand, humidity is another critical parameter affecting performance of the concentrated electrolytes. It may require extra packaging of the

battery when considering their application in some wet areas or seasons. Moreover, the other components of the battery, such as the separators and electrodes, need to be re-designed or carefully selected to better fit the concentrated electrolyte. In line with this, the interaction between the electrode and electrolyte, i.e., the interfaces or the insertion behaviour of ions, needs to be re-visited in the case of concentrated electrolyte. Several publications have mentioned that the insertion behaviour of ions is altered as transforming from diluted to concentrated electrolyte.[235-237] The concentrated LiTFSI lowers the anion-insertion potential in coronene and retrieves more capacity below the onset of oxygen evolution reaction. Many electrode materials which previous were regarded as not-suitable for aqueous batteries may also have an opportunity to revive. Because of the relative sluggish kinetics of ion transportation in the concentrated electrolyte, electrode materials with stable and robust open frameworks, enlarged intercalation channels or layer spacings may be more suitable to fully exert the superiority of the concentrated electrolyte, e.g., the NASICON-type or the PBA cathodes. Organic electrode materials are also potential candidates to be used in the highly concentrated electrolyte as their dissolution in such type of electrolyte can be effectively mitigated. Another concern related with the concentrated electrolytes is their high cost and toxicity. Exploration of inorganic salts with lower cost and large scalability is critical for their wider application. In combination with the state-of-the-art theoretical/simulation methodologies, more fundamental understandings about the ion migration dynamics and atomic-scale interactions between electrolyte and the electrode materials are critical. Last but not least, the stability and voltage of “water-in-salt” should be evaluated in a more practical and standard way, i.e., small amounts of electrolyte, high mass loadings of active materials, and low current rates is needed to allow assessment and comparison of ESW data from different research groups.[238]

Acknowledgements

The authors gratefully acknowledge the National Natural Science Foundation of China (Grant No. 51972067, 21606003, 51802044, 51801030, and 61801314), Guangdong Natural Science Funds for Distinguished Young Scholar (Grant No. 2019B151502039), the 111 project (D18023), Singapore MOE AcRF Tier 2 under Grant Nos. 2018-T2-1-010 and MOE2017-T2-2-069 and National Research Foundation of Singapore (NRF) Investigatorship, award Number NRF2016NRF-NRFI001-22.

References

[1] R. Ruffo, C. Wessells, R.A. Huggins, Y. Cui, Electrochem. Commun. 11 (2009) 247-249.

[2] C. Wessells, R. Ruffo, R.A. Huggins, Y. Cui, Electrochem. Solid-State Lett. 13 (2010) A59-A61.

[3] L. Chen, Z. Guo, Y. Xia, Y. Wang, Chem. Commun. 49 (2013) 2204-2206.

[4] Z. Hou, X. Zhang, X. Li, Y. Zhu, J. Liang, Y. Qian, J. Mater. Chem. A 5 (2017) 730-738.

[5] L. Suo, O. Borodin, T. Gao, M. Olguin, J. Ho, X. Fan, C. Luo, C. Wang, K. Xu, Science 350 (2015) 938-943.

[6] L. Smith, B. Dunn, Science 350 (2015) 918-918.

[7] D.P. Leonard, Z. Wei, G. Chen, F. Du, X. Ji, ACS Energy Lett. 3 (2018) 373-374.

[8] F. Wang, O. Borodin, T. Gao, X. Fan, W. Sun, F. Han, A. Faraone, J.A. Dura, K. Xu, C. Wang, Nat. Mater. 17 (2018) 543-549.

[9] W. Pan, Y. Wang, Y. Zhang, H.Y.H. Kwok, M. Wu, X. Zhao, D.Y.C. Leung, J. Mater. Chem. A 7 (2019) 17420-17425.

[10] V. Verma, S. Kumar, W. Manalastas Jr., R. Satish, M. Srinivasan, Adv. Sustain. Syst. 3 (2019) 1800111.

[11] L. Zhang, L. Chen, X. Zhou, Z. Liu, Adv. Energy Mater. 5 (2015) 1400930.

[12] J.Y. Luo, Y.Y. Xia, Adv. Funct. Mater. 17 (2007) 3877-3884.

[13] D. Kundu, B.D. Adams, V. Duffort, S.H. Vajargah, L.F. Nazar, Nat. Energy 1 (2016) 1-8.

[14] H. Tang, Z. Peng, L. Wu, F. Xiong, C. Pei, Q. An, L. Mai, Electrochem. Energy Rev. 1 (2018) 169-199.

[15] S. Zhang, D. Yang, H. Tan, Y. Feng, X. Rui, Y. Yu, Mater. Today 2020, DOI: 10.1016/j.mattod.2020.03.020.

[16] X. Shan, D.S. Charles, Y. Lei, R. Qiao, G. Wang, W. Yang, M. Feygenson, D. Su, X. Teng, Nat. Commun. 7 (2016) 13370.

[17] C. Yang, J. Chen, X. Ji, T.P. Pollard, X. Lü, C.-J. Sun, S. Hou, Q. Liu, C. Liu, T. Qing, Y. Wang, O. Borodin, Y. Ren, K. Xu, C. Wang, Nature 569 (2019) 245-250.

[18] R. Demir-Cakan, M.R. Palacin, L. Croguennec, J. Mater. Chem. A 7 (2019) 20519-20539.

[19] H. Tan, Y. Feng, X. Rui, Y. Yu, S. Huang, Small Methods 4 (2020) 1900563.

[20] Z. Liu, Y. Huang, Y. Huang, Q. Yang, X. Li, Z. Huang, C. Zhi, Chem. Soc. Rev. 49 (2020) 180-232.

[21] L. Wang, X. Xie, K. Dinh, Q. Yan, J. Ma, Coord. Chem. Rev. 397 (2019) 138-167.

[22] J. Shea, C. Luo, ACS Appl. Mater. Interfaces 12 (2020) 5361-5380.

[23] W. Li, J.R. Dahn, D.S. Wainwright, Science 264 (1994) 1115-1118.

[24] A.S. Lakhnot, T. Gupta, Y. Singh, P. Hundekar, R. Jain, F. Han, N. Koratkar, Energy Storage Mater. 2019, DOI: 10.1016/j.ensm.2019.12.012.

[25] N. Dubouis, P. Lemaire, B. Mirvaux, E. Salager, M. Deschamps, A. Grimaud, Energy Environ. Sci. 11 (2018) 3491-3499.

[26] C.-H. Lin, K. Sun, M. Ge, L.M. Housel, A.H. McCarthy, M.N. Vila, C. Zhao, X. Xiao, W.-K. Lee, K.J. Takeuchi, Sci. Adv. 6 (2020) eaay7129.

[27] Y. Yamada, K. Usui, K. Sodeyama, S. Ko, Y. Tateyama, A. Yamada, Nat. Energy 1 (2016) 16129.

[28] L. Suo, O. Borodin, W. Sun, X. Fan, C. Yang, F. Wang, T. Gao, Z. Ma, M. Schroeder, A. von Cresce, S.M. Russell, M. Armand, A. Angell, K. Xu, C.S. Wang, Angew. Chem. Int. Ed. 55 (2016) 7136-7141.

[29] M.R. Lukatskaya, J.I. Feldblyum, D.G. Mackanic, F. Lissel, D.L. Michels, Y. Cui, Z. Bao, Energy Environ. Sci. 11 (2018) 2876-2883.

[30] O. Borodin, J. Self, K.A. Persson, C. Wang, K. Xu, Joule 4 (2020) 69-100.

[31] Y. Yamada, J. Wang, S. Ko, E. Watanabe, A. Yamada, Nat. Energy 4 (2019) 269-280.

[32] J. Zheng, J.A. Lochala, A. Kwok, Z.D. Deng, J. Xiao, Adv. Sci. 4 (2017) 1700032.

[33] N. Alias, A.A. Mohamad, J. Power Sources 274 (2015) 237-251.

[34] Y. Hou, X. Wang, Y. Zhu, C. Hu, Z. Chang, Y. Wu, R. Holze, J. Mater. Chem. A 1 (2013) 14713-14718.

[35] X. Wang, Q. Qu, Y. Hou, F. Wang, Y. Wu, Chem. Commun. 49 (2013) 6179-6181.

[36] T. Xu, M. Zhao, W. Duan, M. Ding, N.ur R. Lashari, F. Wang, X. Song, Energy Technol. 7 (2019) 1900534.

[37] Y. Wang, S.-Z. Yang, Y. You, Z. Feng, W. Zhu, V. Gariépy, J. Xia, B. Commarieu, A. Darwiche, A. Guerfi, ACS Appl. Mater. Interfaces 10 (2018) 7061-7068.

[38] C. Yang, J. Chen, T. Qing, X. Fan, W. Sun, A. von Cresce, M.S. Ding, O. Borodin, J. Vatamanu, M.A. Schroeder, N. Eidson, C. Wang, K. Xu, Joule 1 (2017) 122-132.

[39] H. Lee, J. Shin, J. W. Choi, Adv. Mater., 30 (2018) 1705851.

[40] Z. Jiang, H. Xie, S. Wang, X. Song, X. Yao, H. Wang, Adv. Energy Mater. 8 (2018) 1801433.

[41] H. Tan, L. Xu, H. Geng, X. Rui, C. Li, S. Huang, Small 14 (2018) 1800567.

[42] D. Chen, H. Tan, X. Rui, Q. Zhang, Y. Feng, H. Geng, C. Li, S. Huang, Y. Yu, InfoMat 1 (2019) 251-259.

[43] H. Chen, D. Yang, X. Zhuang, D. Chen, W. Liu, Q. Zhang, H.H. Hng, X. Rui, Q. Yan, S. Huang, Nano Res. 2019, DOI: 10.1007/s12274-019-2547-9.

[44] D. Yang, Z. Lu, X. Rui, X. Huang, H. Li, J. Zhu, W. Zhang, Y. M. Lam, H. H. Hng, H. Zhang, Q. Yan, Angew. Chem. Int. Ed. 53 (2014) 9352-9355.

[45] D. Chen, X. Rui, Q. Zhang, H. Geng, L. Gan, W. Zhang, C. Li, S. Huang, Y. Yu, Nano Energy 60 (2019) 171-178.

[46] Q. Zhu, S. Zheng, X. Lu, Y. Wan, Q. Chen, J. Yang, L.-z. Zhang, Z. Lu, J. Alloys Compd. 654 (2016) 384-391.

[47] A. Tron, Y.N. Jo, S.H. Oh, Y.D. Park, J. Mun, ACS Appl. Mater. Interfaces 9 (2017) 12391-12399.

[48] Y. Liang, Y. Jing, S. Gheytani, K.-Y. Lee, P. Liu, A. Facchetti, Y. Yao, Nat. Mater. 16 (2017) 841-848.

[49] Y. Sui, C. Liu, R.C. Masse, Z.G. Neale, M. Atif, M. AlSalhi, G. Cao, Energy Storage Mater. 25 (2020) 1-32.

[50] J.M. Wrogemann, S. Künne, A. Heckmann, I.A. Rodríguez-Pérez, V. Siozios, B. Yan, J. Li, M. Winter, K. Beltrop, T. Placke, Adv. Energy Mater. 10 (2020) 1902709.

[51] J. Hao, F. Yang, S. Zhang, H. He, G. Xia, Y. Liu, C. Didier, T. Liu, W.K. Pang, V.K. Peterson, J. Lu, Z. Guo, PNAS 117 (2020) 2815-2823.

[52] N. Zhou, S. Huang, T. Hong, W. Luo, Y. Tian, X. Lu, Z. Zhou, Ceram. Int. 43 (2017) 9327-9333.

[53] Z. Huang, M. Yao, Z. Jiang, W. Meng, B. Li, C. Li, C. Li, Z. He, W. Meng, L. Dai, L. Wang, Solid State Ionics 327 (2018) 123-128.

[54] G. Wu, P. Li, C. Zhu, Y. Lei, H. Zhao, T. Li, H. Yue, B. Dou, Y. Gao, X. Yang, Electrochim. Acta 246 (2017) 720-729.

[55] N. Liu, Z. He, X. Zhang, Y. Jiang, Y. Li, J. Zhu, W. Meng, L. Dai, L. Wang, Ceram. Int. 43 (2017) 11481-11487.

[56] L. Xue, Q. Zhang, X. Zhu, L. Gu, J. Yue, Q. Xia, T. Xing, T. Chen, Y. Yao, H. Xia, Nano Energy 56 (2019) 463-472.

[57] Y. Zhang, P. Xin, Q. Yao, J. Alloys Compd. 741 (2018) 404-408.

[58] Z. Guo, L. Chen, Y. Wang, C. Wang, Y. Xia, ACS Sustainable Chem. Eng. 5 (2017) 1503-1508.

[59] Y. Wen, L. Chen, Y. Pang, Z. Guo, D. Bin, Y. Wang, C. Wang, Y. Xia, ACS Appl. Mater. Interfaces 9 (2017) 8075-8082.

[60] Z. He, Y. Jiang, J. Zhu, H. Wang, Y. Li, H. Zhou, W. Meng, L. Dai, L. Wang, Electrochim. Acta 279 (2018) 279-288.

[61] Z. He, Y. Jiang, J. Zhu, Y. Li, Z. Jiang, H. Zhou, W. Meng, L. Wang, L. Dai, J. Alloys Compd. 731 (2018) 32-38.

[62] F. Wang, L. Suo, Y. Liang, C. Yang, F. Han, T. Gao, W. Sun, C. Wang, Adv. Energy Mater. 7 (2017) 1600922.

[63] C. Yang, X. Ji, X. Fan, T. Gao, L. Suo, F. Wang, W. Sun, J. Chen, L. Chen, F. Han, L. Miao, K. Xu, K. Gerasopoulos, C. Wang, Adv. Mater. 29 (2017) 1701972.

[64] Z. He, Y. Jiang, D. Sun, L. Dai, H. Wang, Ionics 23 (2017) 575-583.

[65] H. Wang, H. Zhang, Y. Cheng, K. Feng, X. Li, H. Zhang, J. Mater. Chem. A 5 (2017) 593-599.

[66] Z. Jiang, Y. Li, J. Zhu, B. Li, C. Li, L. Wang, W. Meng, Z. He, L. Dai, J. Alloys Compd. 791 (2019) 176-183.

[67] G.-M. Weng, L.-Y. Simon Tam, Y.-C. Lu, J. Mater. Chem. A 5 (2017) 11764-11771.

[68] Z. Zhou, W. Luo, H. Huang, S. Huang, Y. Xia, N. Zhou, Z. He, Ceram. Int. 43 (2017) 99-105.

[69] X. Wu, X. Yuan, J. Yu, J. Liu, F. Wang, L. Fu, W. Zhou, Y. Zhu, Q. Zhou, Y. Wu, Nanoscale 9 (2017) 11004-11011.

[70] R. Thimmappa, M. Gautam, S. Aralekallu, M.C. Devendrachari, A.R. Kottaichamy, Z.M. Bhat, M.O. Thotiyl, ChemElectroChem 6 (2019) 2095-2099.

[71] H. Long, W. Zeng, H. Wang, M. Qian, Y. Liang, Z. Wang, Adv. Sci. 5 (2018) 1700634.

[72] K. W. Nam, H. Kim, J. Choi, J. W. Choi, Energy Environ. Sci., 12 (2019), 1999-2009.

[73] C.D. Wessells, M.T. McDowell, S.V. Peddada, M. Pasta, R.A. Huggins, Y. Cui, ACS Nano 6 (2012) 1688-1694.

[74] K. Nakamoto, R. Sakamoto, Y. Sawada, M. Ito, S. Okada, Small Methods 3 (2019) 1800220.

[75] S. Qiu, X. Wu, M. Wang, M. Lucero, Y. Wang, J. Wang, Z. Yang, W. Xu, Q. Wang, M. Gu, Nano Energy 64 (2019) 103941.

[76] H. Wang, T. Zhang, C. Chen, M. Ling, Z. Lin, S. Zhang, F. Pan, C. Liang, Nano Res. 11 (2018) 490-498.

[77] L. Sharma, K. Nakamoto, R. Sakamoto, S. Okada, P. Barpanda, ChemElectroChem 6 (2019) 444-449.

[78] B. Wang, X. Wang, C. Liang, M. Yan, Y. Jiang, ChemElectroChem 6 (2019) 4848-4853.

[79] X. Guo, Z. Wang, Z. Deng, X. Li, B. Wang, X. Chen, S.P. Ong, Chem. Mater. 31 (2019) 5933-5942.

[80] S. Wheeler, I. Capone, S. Day, C. Tang, M. Pasta, Chem. Mater. 31 (2019) 2619-2626.

[81] R.-S. Kühnel, D. Reber, C. Battaglia, ACS Energy Lett. 2 (2017) 2005-2006.

[82] D. Reber, R.-S. Kühnel, C. Battaglia, ACS Mater. Lett. 1 (2019) 44-51.

[83] P. Jiang, Z. Lei, L. Chen, X. Shao, X. Liang, J. Zhang, Y. Wang, J. Zhang, Z. Liu, J. Feng, ACS Appl. Mater. Interfaces 11 (2019) 28762-28768.

[84] J. Han, H. Zhang, A. Varzi, S. Passerini, ChemSusChem 11 (2018) 3704-3707.

[85] K. Nakamoto, R. Sakamoto, M. Ito, A. Kitajou, S. Okada, Electrochem. 85 (2017) 179-185.

[86] M.H. Lee, S.J. Kim, D. Chang, J. Kim, S. Moon, K. Oh, K.-Y. Park, W.M. Seong, H. Park, G. Kwon, Mater. Today 29 (2019) 26-36.

[87] J. Dong, G. Zhang, X. Wang, S. Zhang, C. Deng, J. Mater. Chem. A 5 (2017) 18725-18736.

[88] J.H. Lee, G. Ali, D.H. Kim, K.Y. Chung, Adv. Energy Mater. 7 (2017) 1601491.

[89] B. Paulitsch, J. Yun, A.S. Bandarenka, ACS Appl. Mater. Interfaces 9 (2017) 8107-8112.

[90] F. Yu, S. Zhang, C. Fang, Y. Liu, S. He, J. Xia, J. Yang, N. Zhang, Ceram. Int. 43 (2017) 9960-9967.

[91] Z. Guo, Y. Zhao, Y. Ding, X. Dong, L. Chen, J. Cao, C. Wang, Y. Xia, H. Peng, Y. Wang, Chem 3 (2017) 348-362.

[92] L. Ke, J. Dong, B. Lin, T. Yu, H. Wang, S. Zhang, C. Deng, Nanoscale 9 (2017) 4183-4190.

[93] R. Chua, Y. Cai, Z.K. Kou, R. Satish, H. Ren, J.J. Chan, L. Zhang, S.A. Morris, J. Bai, M. Srinivasan, Chem. Eng. J. 370 (2019) 742-748.

[94] P. Ramesh Kumar, A. Kheireddine, U. Nisar, R.A. Shakoor, R. Essehli, R. Amin, I. Belharouak, J. Power Sources 429 (2019) 149-155.

[95] Y. Qiu, Y. Yu, J. Xu, Y. Liu, M. Ou, S. Sun, P. Wei, Z. Deng, Y. Xu, C. Fang, J. Mater. Chem. A 7 (2019) 24953-24963.

[96] B. He, P. Man, Q. Zhang, C. Wang, Z. Zhou, C. Li, L. Wei, Y. Yao, Small 15 (2019) 1905115.

[97] L. Shen, Y. Jiang, Y. Liu, J. Ma, T. Sun, N. Zhu, Chem. Eng. J. 388 (2020) 124228.

[98] L. Suo, O. Borodin, Y. Wang, X. Rong, W. Sun, X. Fan, S. Xu, M.A. Schroeder, A.V. Cresce, F. Wang, C. Yang, Y.-S. Hu, K. Xu, C. Wang, Adv. Energy Mater. 7 (2017) 1701189.

[99] W. Weng, J. Lin, Y. Du, X. Ge, X. Zhou, J. Bao, J. Mater. Chem. A 6 (2018) 10168-10175.

[100] A.J. Fernández-Ropero, M. Zarrabeitia, M. Reynaud, T. Rojo, M. Casas-Cabanas, J. Phys. Chem. C 122 (2018) 133-142.

[101] M. Morant-Giner, R. Sanchis-Gual, J. Romero, A. Alberola, L. García-Cruz, S. Agouram, M. Galbiati, N.M. Padial, J.C. Waerenborgh, C. Martí-Gastaldo, S. Tatay, A. Forment-Aliaga, E. Coronado, Adv. Funct. Mater. 28 (2018) 1706125.

[102] Q. Yang, S. Cui, Y. Ge, Z. Tang, Z. Liu, H. Li, N. Li, H. Zhang, J. Liang, C. Zhi, Nano Energy 50 (2018) 623-631.

[103] A. Eftekhari, Z. Jian, X. Ji, ACS Appl. Mater. Interfaces 9 (2017) 4404-4419.

[104] Z. Jian, W. Luo, X. Ji, J. Am. Chem. Soc. 137 (2015) 11566-11569.

[105] I. Sultana, T. Ramireddy, M.M. Rahman, Y. Chen, A.M. Glushenkov, Chem. Commun. 52 (2016) 9279-9282.

[106] W. Zhang, J. Mao, S. Li, Z. Chen, Z. Guo, J. Am. Chem. Soc. 139 (2017) 3316-3319.

[107] R.Y. Wang, C.D. Wessells, R.A. Huggins, Y. Cui, Nano Lett. 13 (2013) 5748-5752.

[108] D. Su, A. McDonagh, S.Z. Qiao, G. Wang, Adv. Mater. 29 (2017) 1604007.

[109] C. Li, X. Wang, W. Deng, C. Liu, J. Chen, R. Li, M. Xue, ChemElectroChem 5 (2018) 3887-3892.

[110] B. Huang, Y. Shao, Y. Liu, Z. Lu, X. Lu, S. Liao, ACS Appl. Energy Mater. 2 (2019) 6528-6535.

[111] E. Dražević, A.S. Andersen, K. Wedege, M.L. Henriksen, M. Hinge, A. Bentien, J. Power Sources 381 (2018) 94-100.

[112] C. Liu, T. Ma, K. Xia, X. Hou, Q. Nian, Y. Cai, J. Liang, Sustainable Energy Fuels 4 (2020) 132-137.

[113] L. Jiang, Y. Lu, C. Zhao, L. Liu, J. Zhang, Q. Zhang, X. Shen, J. Zhao, X. Yu, H. Li, Nat. Energy 4 (2019) 495-503.

[114] J. Zhang, Q. Zhou, Y. Tang, L. Zhang, Y. Li, Chem. Sci. 10 (2019) 8924-8929.

[115] C. Wu, H. Tan, W. Huang, W. Li, K. Dinh, C. Yan, W. Wei, L. Chen, Q. Yan, Adv. Funct. Mater. DOI: 10.1002/adfm.202003187.

[116] X. Xie, S. Liang, J. Gao, S. Guo, J. Guo, C. Wang, G. Xu, X. Wu, G. Chen, J. Zhou, Energy Environ. Sci. 13 (2020) 503-510.

[117] J. Shin, J. Lee, Y. Park, J. W. Choi, Chem. Sci., 11 (2020), 2028-2044.

[118] A. Mitha, A.Z. Yazdi, M. Ahmed, P. Chen, ChemElectroChem 5 (2018) 2409-2418.

[119] Y. Wu, Y. Zhang, Y. Ma, J.D. Howe, H. Yang, P. Chen, S. Aluri, N. Liu, Adv. Energy Mater. 8 (2018) 1802470.

[120] Y. Zhang, Y. Wu, H. Ding, Y. Yan, Z. Zhou, Y. Ding, N. Liu, Nano Energy 53 (2018) 666-674.

[121] Z. Zhao, J. Zhao, Z. Hu, J. Li, J. Li, Y. Zhang, C. Wang, G. Cui, Energy Environ. Sci. 12 (2019) 1938-1949.

[122] L. Kang, M. Cui, F. Jiang, Y. Gao, H. Luo, J. Liu, W. Liang, C. Zhi, Adv. Energy Mater. 8 (2018) 1801090.

[123] J. Zheng, Q. Zhao, T. Tang, J. Yin, C.D. Quilty, G.D. Renderos, X. Liu, Y. Deng, L. Wang, D.C. Bock, C. Jaye, D. Zhang, E.S. Takeuchi, K.J. Takeuchi, A.C. Marschilok, L.A. Archer, Science 366 (2019) 645-648.

[124] J.S. Ko, A.B. Geltmacher, B.J. Hopkins, D.R. Rolison, J.W. Long, J.F. Parker, ACS Appl. Energy Mater. 2 (2019) 212-216.

[125] K.E.K. Sun, T.K.A. Hoang, T.N.L. Doan, Y. Yu, X. Zhu, Y. Tian, P. Chen, ACS Appl. Mater. Interfaces 9 (2017) 9681-9687.

[126] Z. Kang, C. Wu, L. Dong, W. Liu, J. Mou, J. Zhang, Z. Chang, B. Jiang, G. Wang, F. Kang, C. Xu, ACS Sustainable Chem. Eng. 7 (2019) 3364-3371.

[127] Y. Liu, Z. Yang, X. Xie, J. Huang, X. Wen, Electrochim. Acta 185 (2015) 190-197.

[128] K.M. McDevitt, D.R. Mumm, A. Mohraz, ACS Appl. Energy Mater. 2 (2019) 8107-8117.

[129] B. Tang, G. Fang, J. Zhou, L. Wang, Y. Lei, C. Wang, T. Lin, Y. Lin, Y. Tang, S. Liang, Nano Energy 51 (2018) 579-587.

[130] J. Shin, D. Choi, H. Lee, Y. Jung, J. W. Choi, Adv. Energy Mater., 9 (2019), 1900083.

[131] G. Fang, J. Zhou, A. Pan, S. Liang, ACS Energy Lett. 3 (2018) 2480-2501.

[132] P. Hu, T. Zhu, X. Wang, X. Wei, M. Yan, J. Li, W. Luo, W. Yang, W. Zhang, L. Zhou, Z. Zhou, L. Mai, Nano Lett. 18 (2018) 1758-1763.

[133] W. Fang, J. Zhao, T. Wu, Y. Huang, L. Yang, C. Liu, Q. Zhang, K. Huang, Q. Yan, J. Mater. Chem. A, 8 (2020) 5913-5918.

[134] X. Liu, H. Zhang, D. Geiger, J. Han, A. Varzi, U. Kaiser, A. Moretti, S. Passerini, Chem. Commun. 55 (2019) 2265-2268.

[135] J. He, X. Liu, H. Zhang, Z. Yang, X. Shi, Q. Liu, X. Lu, ChemSusChem 13 (2020) 1568-1574.

[136] B. Tang, J. Zhou, G. Fang, S. Guo, X. Guo, L. Shan, Y. Tang, S. Liang, J. Electrochem. Soc. 166 (2019) A480-A486.

[137] B. Lan, Z. Peng, L. Chen, C. Tang, S. Dong, C. Chen, M. Zhou, C. Chen, Q. An, P. Luo, J. Alloys Compd. 787 (2019) 9-16.

[138] L. Ma, N. Li, C. Long, B. Dong, D. Fang, Z. Liu, Y. Zhao, X. Li, J. Fan, S. Chen, Adv. Funct. Mater. 29 (2019) 1906142.

[139] W. Yang, L. Dong, W. Yang, C. Xu, G. Shao, G. Wang, Small Methods 4 (2020) 1900670.

[140] R. Li, H. Zhang, Q. Zheng, X. Li, J. Mater. Chem. A 8 (2020) 5186-5193.

[141] J. Wang, J.-G. Wang, H. Liu, Z. You, C. Wei, F. Kang, J. Power Sources 438 (2019) 226951.

[142] J. Huang, Z. Wang, M. Hou, X. Dong, Y. Liu, Y. Wang, Y. Xia, Nat. Commun. 9 (2018) 2906.

[143] G. Fang, C. Zhu, M. Chen, J. Zhou, B. Tang, X. Cao, X. Zheng, A. Pan, S. Liang, Adv. Funct. Mater. 29 (2019) 1808375.

[144] H. Ren, J. Zhao, L. Yang, Q. Liang, S. Madhavi, Q. Yan, Nano Res. 12 (2019) 1347-1353.

[145] L. Ma, S. Chen, H. Li, Z. Ruan, Z. Tang, Z. Liu, Z. Wang, Y. Huang, Z. Pei, J.A. Zapien, C. Zhi, Energy Environ. Sci. 11 (2018) 2521-2530.

[146] R. Trócoli, F. La Mantia, ChemSusChem 8 (2015) 481-485.

[147] X. Wu, Y. Xu, C. Zhang, D.P. Leonard, A. Markir, J. Lu, X. Ji, J. Am. Chem. Soc. 141 (2019) 6338-6344.

[148] Q. Zhao, W. Huang, Z. Luo, L. Liu, Y. Lu, Y. Li, L. Li, J. Hu, H. Ma, J. Chen, Sci. Adv. 4 (2018) eaao1761.

[149] X. Yue, H. Liu, P. Liu, Chem. Commun. 55 (2019) 1647-1650.

[150] K.W. Nam, H. Kim, Y. Beldjoudi, T.-w. Kwon, D.J. Kim, J.F. Stoddart, J. Am. Chem. Soc. 142 (2020) 2541-2548.

[151] Z. Guo, Y. Ma, X. Dong, J. Huang, Y. Wang, Y. Xia, Angew. Chem. Int. Ed. 57 (2018) 11737-11741.

[152] P. Hu, T. Zhu, J. Ma, C. Cai, G. Hu, X. Wang, Z. Liu, L. Zhou, L. Mai, Chem. Commun. 55 (2019) 8486-8489.

[153] J. Zhao, H. Ren, Q. Liang, D. Yuan, S. Xi, C. Wu, W. Manalastas, J. Ma, W. Fang, Y. Zheng, C.-F. Du, M. Srinivasan, Q. Yan, Nano Energy 62 (2019) 94-102.

[154] X. Chen, L. Wang, H. Li, F. Cheng, J. Chen, J. Energy Chem. 38 (2019) 20-25.

[155] Z. Li, S. Ganapathy, Y. Xu, Z. Zhou, M. Sarilar, M. Wagemaker, Adv. Energy Mater. 9 (2019) 1900237.

[156] B. Sambandam, V. Soundharrajan, S. Kim, M.H. Alfaruqi, J. Jo, S. Kim, V. Mathew, Y.-k. Sun, J. Kim, J. Mater. Chem. A 6 (2018) 3850-3856.

[157] N. Zhang, Y. Dong, M. Jia, X. Bian, Y. Wang, M. Qiu, J. Xu, Y. Liu, L. Jiao, F. Cheng, ACS Energy Lett. 3 (2018) 1366-1372.

[158] V. Soundharrajan, B. Sambandam, S. Kim, M.H. Alfaruqi, D.Y. Putro, J. Jo, S. Kim, V. Mathew, Y.-K. Sun, J. Kim, Nano Lett. 18 (2018) 2402-2410.

[159] X. Chu, H. Wang, Y. Chi, C. Wang, L. Lei, W. Zhang, X. Yang, RSC Adv. 8 (2018) 2072-2076.

[160] Q. Pang, C. Sun, Y. Yu, K. Zhao, Z. Zhang, P.M. Voyles, G. Chen, Y. Wei, X. Wang, Adv. Energy Mater. 8 (2018) 1800144.

[161] Y. Cai, F. Liu, Z. Luo, G. Fang, J. Zhou, A. Pan, S. Liang, Energy Storage Mater. 13 (2018) 168-174.

[162] B. Tang, J. Zhou, G. Fang, F. Liu, C. Zhu, C. Wang, A. Pan, S. Liang, J. Mater. Chem. A 7 (2019) 940-945.

[163] P. He, G. Zhang, X. Liao, M. Yan, X. Xu, Q. An, J. Liu, L. Mai, Adv. Energy Mater. 8 (2018) 1702463.

[164] B. Wu, G. Zhang, M. Yan, T. Xiong, P. He, L. He, X. Xu, L. Mai, Small 14 (2018) 1703850.

[165] Z. Guo, Y. Ma, X. Dong, J. Huang, Y. Wang, Y. Xia, Angew. Chem. Int. Ed. 130 (2018) 11911-11915.

[166] H. Qin, Z. Yang, L. Chen, X. Chen, L. Wang, J. Mater. Chem. A 6 (2018) 23757-23765.

[167] H. Li, Q. Yang, F. Mo, G. Liang, Z. Liu, Z. Tang, L. Ma, J. Liu, Z. Shi, C. Zhi, Energy Storage Mater. 19 (2019) 94-101.

[168] D. Aurbach, Z. Lu, A. Schechter, Y. Gofer, H. Gizbar, R. Turgeman, Y. Cohen, M. Moshkovich, E. Levi, Nature 407 (2000) 724-727.

[169] J. Muldoon, C.B. Bucur, A.G. Oliver, T. Sugimoto, M. Matsui, H.S. Kim, G.D. Allred, J. Zajicek, Y. Kotani, Energy Environ. Sci. 5 (2012) 5941-5950.

[170] O. Mizrahi, N. Amir, E. Pollak, O. Chusid, V. Marks, H. Gottlieb, L. Larush, E. Zinigrad, D. Aurbach, J. Electrochem. Soc. 155 (2008) A103-A109.

[171] X. Sun, V. Duffort, B.L. Mehdi, N.D. Browning, L.F. Nazar, Chem. Mater. 28 (2016) 534-542.

[172] M. Deng, L. Wang, D. Höche, S.V. Lamaka, D. Snihirova, B. Vaghefinazari, M.L. Zheludkevich, J. Power Sources 441 (2019) 227201.

[173] J. Xu, Z. Wei, L. Tang, A. Wang, Y. Zhang, Y. Qiao, C. Chen, J. Power Sources 454 (2020) 227869.

[174] T. Cain, C. Glover, J. Scully, Electrochim. Acta 297 (2019) 564-575.

[175] X. Liu, S. Liu, J. Xue, J. Power Sources 396 (2018) 667-674.

[176] H. Xiong, H. Zhu, J. Luo, K. Yu, C. Shi, H. Fang, Y. Zhang, J. Mater. Eng. Perform. 26 (2017) 2901-2911.

[177] S. Yuan, H. Lu, Z. Sun, L. Fan, X. Zhu, W. Zhang, J. Electrochem. Soc. 163 (2016) A1181-A1187.

[178] Y. Feng, W. Xiong, J. Zhang, R. Wang, N. Wang, J. Mater. Chem. A 4 (2016) 8658-8668.

[179] Y. Lv, M. Liu, Y. Xu, D. Cao, J. Feng, R. Wu, M. Zhang, J. Power Sources 239 (2013) 265-268.

[180] T.W. Cain, C.F. Glover, J.R. Scully, Electrochim. Acta 297 (2019) 564-575.

[181] J.A. Yuwono, N. Birbilis, K.S. Williams, N.V. Medhekar, J. Phys. Chem. C 120 (2016) 26922-26933.

[182] H. Zhang, K. Ye, K. Zhu, R. Cang, J. Yan, K. Cheng, G. Wang, D. Cao, Chem. Eur. J. 23 (2017) 17118-17126.

[183] H. Zhang, K. Ye, K. Zhu, R. Cang, J. Yan, K. Cheng, G. Wang, D. Cao, Electrochim. Acta 256 (2017) 357-364.

[184] F. Wang, X. Fan, T. Gao, W. Sun, Z. Ma, C. Yang, F. Han, K. Xu, C. Wang, ACS Cent. Sci. 3 (2017) 1121-1128.

[185] L. Chen, J.L. Bao, X. Dong, D.G. Truhlar, Y. Wang, C. Wang, Y. Xia, ACS Energy Lett. 2 (2017) 1115-1121.

[186] J.-S. Kim, W.-S. Chang, R.-H. Kim, D.-Y. Kim, D.-W. Han, K.-H. Lee, S.-S. Lee, S.-G. Doo, J. Power Sources 273 (2015) 210-215.

[187] C. Kim, P.J. Phillips, B. Key, T. Yi, D. Nordlund, Y.S. Yu, R.D. Bayliss, S.D. Han, M. He, Z. Zhang, Adv. Mater. 27 (2015) 3377-3384.

[188] S. Tao, W. Huang, Y. Liu, S. Chen, B. Qian, L. Song, J. Mater. Chem. A 6 (2018) 8210-8214.

[189] Y. Cho, M.H. Lee, H. Kim, K. Ku, G. Yoon, S.-K. Jung, B. Lee, J. Kim, K. Kang, Mater. Res. Bull. 96 (2017) 524-532.

[190] H. Zhang, K. Ye, X. Huang, X. Wang, K. Cheng, X. Xiao, G. Wang, D. Cao, J. Power Sources 338 (2017) 136-144.

[191] H. Zhang, K. Ye, K. Zhu, R. Cang, X. Wang, G. Wang, D. Cao, ACS Sustainable Chem. Eng. 5 (2017) 6727-6735.

[192] G. Liu, Q. Chi, Y. Zhang, Q. Chen, C. Zhang, K. Zhu, D. Cao, Chem. Commun. 54 (2018) 9474-9477.

[193] Z. Jia, J. Hao, L. Liu, Y. Wang, T. Qi, Ionics 24 (2018) 3483-3491.

[194] H. Zhang, D. Cao, X. Bai, H. Xie, X. Liu, X. Jiang, H. Lin, H. He, ACS Sustainable Chem. Eng. 7 (2019) 6113-6121.

[195] X. Cao, L. Wang, J. Chen, J. Zheng, ChemElectroChem 5 (2018) 2789-2794.

[196] H. Zhang, K. Ye, R. Cang, K. Zhu, J. Yan, K. Cheng, G. Wang, D. Cao, J. Electroanal. Chem. 807 (2017) 37-44.

[197] P. Shan, Y. Gu, L. Yang, T. Liu, J. Zheng, F. Pan, Inorg. Chem. 56 (2017) 13411-13416.

[198] Y. Zhang, G. Liu, C. Zhang, Q. Chi, T. Zhang, Y. Feng, K. Zhu, Y. Zhang, Q. Chen, D. Cao, Chem. Eng. J. 392 (2020) 123652.

[199] J. Xu, Y. Dou, Z. Wei, J. Ma, Y. Deng, Y. Li, H. Liu, S. Dou, Adv. Sci. 4 (2017) 1700146.

[200] N. Jayaprakash, S.K. Das, L.A. Archer, Chem. Commun. 47 (2011) 12610-12612.

[201] M.-C. Lin, M. Gong, B. Lu, Y. Wu, D.-Y. Wang, M. Guan, M. Angell, C. Chen, J. Yang, B.-J. Hwang, H. Dai, Nature 520 (2015) 324-328.

[202] Z. Hu, Y. Guo, H. Jin, H. Ji, L.-J. Wan, Chem. Commun. 56 (2020) 2023-2026.

[203] H. Yang, H. Li, J. Li, Z. Sun, K. He, H.-M. Cheng, F. Li, Angew. Chem. Int. Ed. 58 (2019) 11978-11996.

[204] G.A. Elia, K. Marquardt, K. Hoeppner, S. Fantini, R. Lin, E. Knipping, W. Peters, J.-F. Drillet, S. Passerini, R. Hahn, Adv. Mater. 28 (2016) 7564-7579.

[205] Y. Hu, D. Sun, B. Luo, L. Wang, Energy Technol. 7 (2019) 86-106.

[206] Q. Zhao, M.J. Zachman, W.I. Al Sadat, J. Zheng, L.F. Kourkoutis, L. Archer, Sci. Adv. 4 (2018) eaau8131.

[207] S. He, J. Wang, X. Zhang, J. Chen, Z. Wang, T. Yang, Z. Liu, Y. Liang, B. Wang, S. Liu, Adv. Funct. Mater. 29 (2019) 1905228.

[208] J. Joseph, J. Nerkar, C. Tang, A. Du, A.P. O'Mullane, K. Ostrikov, ChemSusChem 12 (2019) 3753-3760.

[209] S. Nandi, S.K. Das, ACS Sustainable Chem. Eng. 7 (2019) 19839-19847.

[210] S. Liu, J.J. Hu, N.F. Yan, G.L. Pan, G.R. Li, X.P. Gao, Energy Environ. Sci. 5 (2012) 9743-9746.

[211] Z. Li, K. Xiang, W. Xing, W.C. Carter, Y.-M. Chiang, Adv. Energy Mater. 5 (2015) 1401410.

[212] M.L. Agiorgousis, Y.-Y. Sun, S. Zhang, ACS Energy Lett. 2 (2017) 689-693.

[213] Y. Hu, B. Luo, D. Ye, X. Zhu, M. Lyu, L. Wang, Adv. Mater. 29 (2017) 1606132.

[214] S. Wang, Z. Yu, J. Tu, J. Wang, D. Tian, Y. Liu, S. Jiao, Adv. Energy Mater. 6 (2016) 1600137.

[215] H. Wang, X. Bi, Y. Bai, C. Wu, S. Gu, S. Chen, F. Wu, K. Amine, J. Lu, Adv. Energy Mater. 7 (2017) 1602720.

[216] S. Wang, S. Jiao, J. Wang, H.-S. Chen, D. Tian, H. Lei, D.-N. Fang, ACS Nano 11 (2017) 469-477.

[217] Z. Yu, Z. Kang, Z. Hu, J. Lu, Z. Zhou, S. Jiao, Chem. Commun. 52 (2016) 10427-10430.

[218] C. Wu, S. Gu, Q. Zhang, Y. Bai, M. Li, Y. Yuan, H. Wang, X. Liu, Y. Yuan, N. Zhu, Nat. Commun. 10 (2019) 1-10.

[219] Y. Liu, C. Li, J. Xu, M. Ou, C. Fang, S. Sun, Y. Qiu, J. Peng, G. Lu, Q. Li, J. Han, Y. Huang, Nano Energy 67 (2020) 104211.

[220] Y.-S. Kim, K.D. Harris, B. Limoges, V. Balland, Chem. Sci. 10 (2019) 8752-8763.

[221] A. Zhou, L. Jiang, J. Yue, Y. Tong, Q. Zhang, Z. Lin, B. Liu, C. Wu, L. Suo, Y.-S. Hu, H. Li, L. Chen, ACS Appl. Mater. Interfaces 11 (2019) 41356-41362.

[222] S. Nandi, S.K. Das, Solid State Ionics 347 (2020) 115228.

[223] P. Wang, Z. Chen, Z. Ji, Y. Feng, J. Wang, J. Liu, M. Hu, H. Wang, W. Gan, Y. Huang, Chem. Eng. J. 373 (2019) 580-586.

[224] F. Nacimiento, M. Cabello, R. Alcántara, P. Lavela, J.L. Tirado, Electrochim. Acta 260 (2018) 798-804.

[225] Q. Zhao, L. Liu, J. Yin, J. Zheng, D. Zhang, J. Chen, L.A. Archer, Angew. Chem. Int. Ed. 59 (2020) 3048-3052.

[226] W. Pan, Y. Wang, Y. Zhang, H.Y.H. Kwok, M. Wu, X. Zhao, D.Y. Leung, J. Mater. Chem. A 7 (2019) 17420-17425.

[227] C. Wu, S. Gu, Q. Zhang, Y. Bai, M. Li, Y. Yuan, H. Wang, X. Liu, Y. Yuan, N. Zhu, F. Wu, H. Li, L. Gu, J. Lu, Nat. Commun. 10 (2019) 73.

[228] H. Lahan, S.K. Das, J. Power Sources 413 (2019) 134-138.

[229] S. Kumar, R. Satish, V. Verma, H. Ren, P. Kidkhunthod, W. Manalastas, M. Srinivasan, J. Power Sources 426 (2019) 151-161.

[230] M. Kazazi, Z.A. Zafar, M. Delshad, J. Cervenka, C. Chen, Solid State Ionics 320 (2018) 64-69.

[231] Y. Ru, S. Zheng, H. Xue, H. Pang, Chem. Eng. J. 382 (2020) 122853.

[232] D. Chao, C. Ye, F. Xie, W. Zhou, Q. Zhang, Q. Gu, K. Davey, L. Gu, S. Qiao, Adv. Mater. (2020) 2001894.

[233] D. Chao, W. Zhou, C. Ye, Q. Zhang, Y. Chen, L. Gu, K. Davey, S. Qiao, Angew. Chem. Int. Ed., 58 (2019) 7823-7828.

[234] M. Ng, J. Zhao, Q. Yan, G. Conduit, Z. Seh, Nat. Mach. Intell. 2 (2020) 161–170.

[235] I.A. Rodríguez-Pérez, L. Zhang, D.P. Leonard, X. Ji, Electrochem. Commun. 109 (2019) 106599.

[236] Y. Kondo, Y. Miyahara, T. Fukutsuka, K. Miyazaki, T. Abe, Electrochem. Commun. 100 (2019) 26-29.

[237] L. Zhang, I.A. Rodríguez-Pérez, H. Jiang, C. Zhang, D.P. Leonard, Q. Guo, W. Wang, S. Han, L. Wang, X. Ji, Adv. Funct. Mater. 29 (2019) 1902653.

[238] R.-S. Kühnel, D. Reber, C. Battaglia, J. Electrochem. Soc. 167 (2020) 070544.